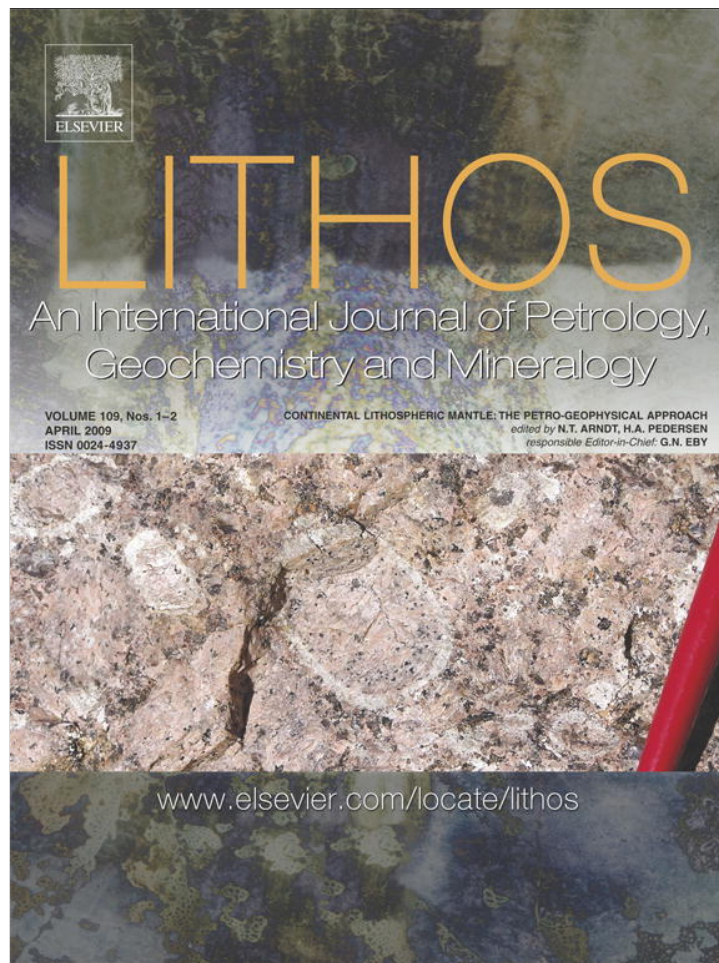


Provided for non-commercial research and education use.  
Not for reproduction, distribution or commercial use.



This article appeared in a journal published by Elsevier. The attached copy is furnished to the author for internal non-commercial research and education use, including for instruction at the authors institution and sharing with colleagues.

Other uses, including reproduction and distribution, or selling or licensing copies, or posting to personal, institutional or third party websites are prohibited.

In most cases authors are permitted to post their version of the article (e.g. in Word or Tex form) to their personal website or institutional repository. Authors requiring further information regarding Elsevier's archiving and manuscript policies are encouraged to visit:

<http://www.elsevier.com/copyright>



Contents lists available at ScienceDirect

Lithos

journal homepage: [www.elsevier.com/locate/lithos](http://www.elsevier.com/locate/lithos)

## Seismic structure of Precambrian lithosphere: New constraints from broad-band surface-wave dispersion

Sergei Lebedev<sup>a,b,\*</sup>, Jan Boonen<sup>b</sup>, Jeannot Trampert<sup>b</sup>

<sup>a</sup> Dublin Institute for Advanced Studies, School of Cosmic Physics, Geophysics Section, 5 Merrion Square, Dublin 2, Ireland

<sup>b</sup> Utrecht University, Department of Earth Sciences, Budapestlaan 4, Utrecht, 3584 CD, The Netherlands

### ARTICLE INFO

#### Article history:

Received 4 June 2008

Accepted 11 June 2008

Available online 26 June 2008

#### Keywords:

Shear-wave

Radial anisotropy

Craton

Archean

Proterozoic

Hales discontinuity

### ABSTRACT

Depth distributions of seismic velocities and their directional dependence (anisotropy) in the crust and mantle beneath cratons yield essential constraints on processes of their formation and evolution. Despite recent progress in mapping the lateral extent of cratonic roots around the globe, profiles of seismic velocities within them remain uncertain. In this study we employ a novel combination of waveform-analysis techniques and measure inter-station Rayleigh- and Love-wave phase velocities in broad period ranges that enable resolution from the upper crust to deep upper mantle. Sampling a selection of 10 Archean and Proterozoic locations, we derive new constraints on the isotropic and radially anisotropic seismic structure of Precambrian lithosphere.

Shear-wave speed  $V_S$  is consistently higher in the lithosphere of cratons than in the lithosphere of Proterozoic foldbelts. Because known effects of compositional variations in the lithosphere on  $V_S$  are too small to account for the difference, this implies that temperature in cratonic lithosphere is consistently lower, in spite of sub-lithospheric mantle beneath continents being thermally heterogeneous, with some cratons underlain, as we observe, by a substantially hotter asthenosphere compared to others. Lithospheric geotherms being nearly conductive, this confirms that the stable, buoyant lithosphere beneath cratons must be substantially thicker than beneath younger continental blocks.

An increase in  $V_S$  between the Moho and a 100–150 km depth is consistently preferred by the data in this study and is present in seismic models of continents published previously. We argue that this is largely due to the transition from spinel peridotite to garnet peridotite, proposed previously to give rise to the “Hales discontinuity” within this depth interval. The depth and the width of the phase transformation depend on mantle composition; it is likely to occur deeper and over a broader depth interval beneath cratons than elsewhere because of the high Cr content in the depleted cratonic lithosphere, as evidenced by a number of xenolith studies. Seismic data available at present would be consistent with both a sharp and a gradual increase in  $V_S$  in the upper lithosphere (a Hales discontinuity or a “Hales gradient”). The  $V_S$  profile in the upper mantle lithosphere is not shaped by the temperature distribution only; this needs to be considered when relating seismic velocities to lithospheric temperatures.

Radial anisotropy in the upper crust is observed repeatedly and indicates vertically oriented anisotropic fabric ( $V_{SH} < V_{SV}$ ); this may yield a clue on how cratons grew, lending support to the view that distributed crustal shortening with sub-vertical flow patterns occurred over large scales in hot ancient orogens. In the lower crust and upper lithospheric mantle, radial anisotropy consistently reveals horizontal fabric ( $V_{SH} > V_{SV}$ ); the fabric can be interpreted as a record of (sub-)horizontal ductile flow in the lower crust and lithospheric mantle at the time of the formation and stabilisation of the cratons. We also find indications for radial anisotropy below 200 km depth, corroborating recent evidence for anisotropy in the asthenosphere beneath cratons due to current and recent asthenospheric flow.

© 2008 Elsevier B.V. All rights reserved.

### 1. Introduction

Seismic properties of the cratonic lithosphere reflect its composition and physical state and yield basic constraints on the architecture

of cratons, on processes of their formation, and on the causes for their stability. It has long been recognised that cratons are underlain by a thick, high-velocity seismic lithosphere (Brune and Dorman, 1963; Jordan, 1975; Grand and Helmlinger, 1984). Recently, seismic tomography has been producing increasingly accurate maps of the locations and boundaries of the seismically “fast” cratonic lithosphere (e.g. Zielhuis and Nolet, 1994; Van der Lee and Nolet, 1997; Frederiksen et al., 2001; Shapiro and Ritzwoller, 2002; Simons et al.,

\* Corresponding author. Dublin Institute for Advanced Studies, School of Cosmic Physics, Geophysics Section, 5 Merrion Square, Dublin 2, Ireland.  
E-mail address: [sergei@cp.dias.ie](mailto:sergei@cp.dias.ie) (S. Lebedev).

2002; Gung et al., 2003; Lebedev and Nolet, 2003; Ritsema et al., 2004; Yoshizawa and Kennett, 2004; Debayle et al., 2005; Fishwick et al., 2005; Chevrot and Zhao, 2007; Lebedev and van der Hilst, 2008) (Fig. 1). The distribution of seismic velocities with depth, however, is still uncertain, and even its most basic properties are disputed: do seismic velocities increase or decrease in the mantle lithosphere below the crust–mantle interface (the Moho)? What are the ranges of seismic-velocity values within cratonic lithosphere? Where does the lithosphere bottom? Is there a low-velocity zone below? What is the anisotropy within and below cratonic lithosphere?

Solutions of seismic inverse problems are non-unique and have substantial uncertainties. The uncertainties, moreover, can be difficult to quantify, in particular in the case of large-scale tomographic problems. An example of a current debate unresolved due, in part, to the uncertainties of seismic models being too large is one concerning the gradient in seismic velocities between the Moho and a 100–150 km depth. In many published three-dimensional (3D) models and one-dimensional (1D) profiles (e.g. Paulssen, 1987; Gaherty and Jordan, 1995; Ekström, 2000; Freybourger et al., 2001; Lebedev and Nolet, 2003; Bruneton et al., 2004; Fishwick and Reading, 2008) there is an increase in the shear-wave speed ( $V_S$ ) beneath stable continents between the Moho and a 100–150 km depth. Surface-wave observations can be expected to enable us to determine accurately gradients in  $V_S$  over such depth intervals. Seismic models, however, are non-unique (a range of models will fit the data within error bars), and it has been argued recently that surface-wave data can also be matched with

models in which  $V_S$  decreases monotonically below the Moho (Shapiro and Ritzwoller, 2004). If mantle lithosphere was made up of roughly the same material at all depths then such a negative gradient would be expected: lithospheric seismic-velocity anomalies would be primarily of thermal origin, and temperature—according to realistic geotherms for this thermal boundary layer—rises rapidly and monotonically with depth within the lithosphere, which implies a decrease in seismic velocities with depth. The point in question is thus whether the lithospheric rock is indeed the same at different depths or, instead, changes with depth in its physical properties.

The depth and the seismic expression of the bottom of cratonic lithosphere are also disputed (e.g. Eaton et al., 2009–this issue), as are the absolute values of seismic velocities in the lithosphere and the presence of a low-velocity zone beneath cratons (e.g. Freybourger et al., 2001). Tighter constraints on these features are needed to advance our understanding of the mechanism of the stability of cratons.

Seismic anisotropy within the lithosphere of stable cratons reflects the fabric created at the time when they experienced strong deformation, during their formation and stabilisation. Most workers report radial anisotropy in cratonic mantle lithosphere that is indicative of horizontally oriented fabric ( $V_{SH} > V_{SV}$ ) (e.g. Gaherty and Jordan, 1995; Beghein and Trampert, 2003), but some models suggested the presence of vertical fabric ( $V_{SH} < V_{SV}$ ) (Babuška et al., 1998), which has recently been interpreted as evidence for a hypothetical large enhancement in vertical thermal conductivity in Archean lithosphere that could have contributed significantly to the

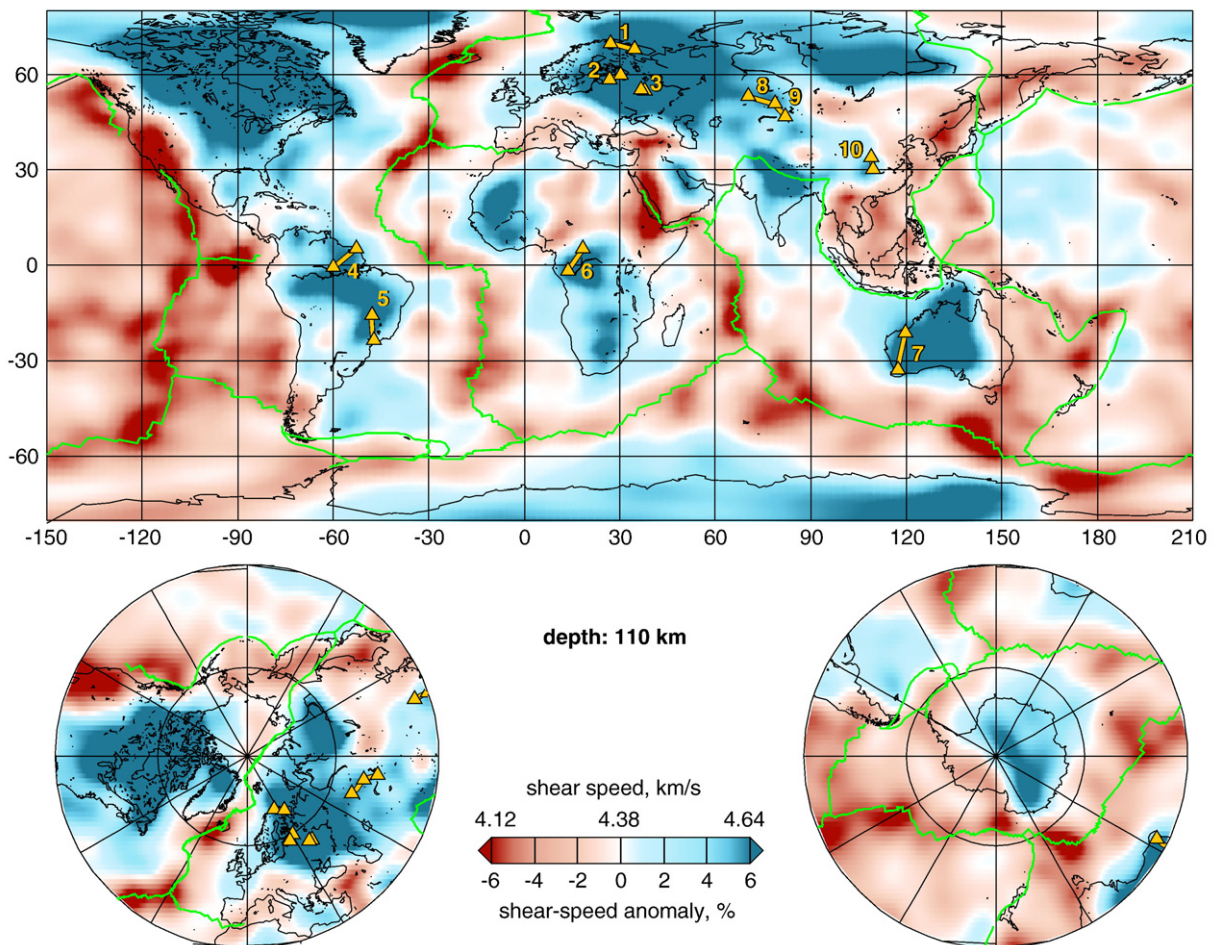


**Fig. 1.** The ten station pairs (triangles) and the inter-station paths selected for surface-wave dispersion measurements (Table 1), plotted on the background of shear-wave speeds at a 110 km depth in the mantle according to the tomographic model of Lebedev and van der Hilst (2008). The reference period of the tomographic model is 50 s. Almost all prominent high-velocity anomalies (blue) show stable Precambrian lithospheres (exceptions being high-velocity subducting lithospheres in subduction zones).

stabilisation of cratonic roots (Petitjean et al., 2006). Horizontal fabric in the lower continental crust is thought to be a record of sub-horizontal ductile flow during past deformation episodes (Meissner et al., 2006). In the upper crust, craton-scale (or orogen-scale) radial anisotropy is poorly known.

In this study we perform elaborate inter-station measurements of surface-wave phase velocities in broad period ranges. Sampling a selection of 10 Archean and Proterozoic locations, we derive new constraints on both isotropic and radially anisotropic seismic structure of Precambrian lithosphere.

The fundamental advantage of inter-station measurements of surface-wave phase velocities—compared to the “earthquake-station” measurements used, in particular, in large-scale tomography—is that they can be performed, in principle, in broader frequency bands. Recently, Lebedev et al. (2006) have used a novel combination of waveform-analysis techniques to measure Rayleigh- and Love-wave dispersion (frequency dependence of phase velocities) in a very broad period range of 8–340 s. Surface waves at different periods are sensitive to elastic properties in different depth ranges; measuring Rayleigh- and Love-wave dispersion over broad period ranges (including, in particular, short periods of 10–20 s) enables one to resolve trade-offs between model parameters in the crust and in the upper mantle and, thus, determine isotropic and anisotropic seismic structure of both the crust and the mantle with a substantially higher accuracy, compared to more conventional, narrower-band measurements.

Another advantage of inter-station dispersion analysis is that a local shear-velocity profile (characterizing the average seismic structure beneath the station pair) can be obtained from phase-velocity data by solving a small, simple inverse problem. Using series of straightforward tests, the relatively simple model space of the inverse problem can be explored in sufficient detail so as to derive robust conclusions on the ranges of seismic structure parameters that are consistent with the data.

## 2. The Precambrian units sampled

We aimed to obtain tight constraints on  $V_S$  profiles beneath a selection of Precambrian units, in order to derive inferences on the structure of Precambrian lithosphere in general. We thus wished to measure dispersion curves in as broad frequency bands as possible, with as small uncertainties as possible, and sampling a number of

different cratons. We opted to use seismic stations only from the Global Seismographic Network (GSN) and GEOFON. The two global networks use the most advanced types of seismographs as well as elaborate installations; they also include pairs of stations situated close enough to each other for our purposes.

We chose pairs of GSN and GEOFON stations such that the inter-station paths were underlain by high-velocity lithosphere, according to high-resolution global tomography (Fig. 1). Due to surface-wave diffraction, it is difficult to measure dispersion accurately at short periods (<25 s) when inter-station distances are longer than  $\sim 10^\circ$ . The inter-station distances are thus up to  $10^\circ$ , the only exception being the longer path that traverses Western Australia (Table 1).

Short-period surface waves (periods below  $\sim 25$  s) sample the continental-crust depth range and are necessary in order to distinguish seismic anomalies in the crust from those in the uppermost mantle. This is because longer-period data are sensitive to both crustal and mantle structure, so that they alone are consistent with much broader ranges of mantle models. For example, without short-period data it is sometimes possible to attribute observed surface-wave anisotropy either entirely to anisotropy in the crust or entirely to anisotropy in the mantle lithosphere, with acceptable fit to data for both types of models. A conservative interpretation of such data may have to be that we simply cannot tell whether there is any anisotropy in the lithospheric mantle and whether there is any anisotropy in the crust. We, therefore, aim to utilise as much short-period data as possible, and this imposes an upper limit on inter-station distances.

Using the two requirements—that stations of a pair are situated both close to each other and atop high-velocity lithosphere (Fig. 1)—we were able to select ten station pairs (Table 1). Two of the stations were replaced at some dates by stations named differently but at locations nearby (TRTE/VSU; KOG/MPG); we used data from both the earlier and the later deployments.

From a geological point of view, the choice of Precambrian units sampled in this study is random. In Europe, one inter-station path traverses the Archean Baltic Shield and two paths sample the Archean–Proterozoic Russian Platform (Artemieva et al., 2006). In South America, one path is across the Archean Guyana Shield and another across the Paraná Basin.

The Paraná Basin is covered with thick Phanerozoic sediments, but its seismic lithosphere has structure similar to that beneath Precambrian cratons, according both to tomography (Fig. 1) and to

**Table 1**  
The data set: station pairs, station coordinates, inter-station distances  $\Delta$ , tectonic units sampled, the numbers of events ( $N_e$ ) and the period ranges ( $T$ ) for Rayleigh (R) and Love (L) waves

No.	Stations	Latitude	Longitude	$\Delta$ , km	Site	Age	$N_e$ (R)	$N_e$ (L)	$T$ (R), s	$T$ (L), s
1	KEV–	69.76°N	27.01°E	369	Baltic Shield	Archean	236	117	11–400	8–143
	–LVZ	67.90°N	34.65°E							
2	PUL–	59.77°N	30.32°E	257	Russian Platform	Arch./Prot.	230	44	8–125	9–50
	–TRTE	58.38°N	26.72°E							
	–VSU	58.46°N	26.73°E							
3	MHV–	54.96°N	37.77°E	78	Russian Platform	Arch./Prot.	133	73	15–125	14–54
	–OBN	55.11°N	36.57°E							
4	PTGA–	0.73°S	59.97°W	1038	Guyana Shield	Archean	42	28	19–222	17–59
	–KOG	5.21°N	52.73°W							
	–MPG	5.11°N	52.64°W							
5	BDFB–	15.64°S	48.01°W	884	Paraná Basin	Arch./Prot.	29	11	17–105	17–43
	–SPB	23.59°S	47.43°W							
6	BGCA–	5.18°N	18.42°E	927	Congo Craton	Archean	16	4	17–77	22–34
	–MSKU	1.66°S	13.61°E							
7	MBWA–	21.16°S	119.73°E	1329	Western Australia	Archean	146	84	26–333	26–200
	–NWA0	32.93°S	117.23°E							
8	BRVK–	53.06°N	70.28°E	627	Kazakhstan	Proterozoic	223	26	13–400	14–51
	–KURK	50.72°N	78.62°E							
9	KURK–	50.72°N	78.62°E	498	Kazakhstan	Proterozoic	111	28	13–286	21–51
	–MAKZ	46.81°N	81.98°E							
10	ENH–	30.27°N	109.49°E	421	Yangtze Craton	Proterozoic	102	43	9–333	13–47
	–XAN	34.03°N	108.92°E							

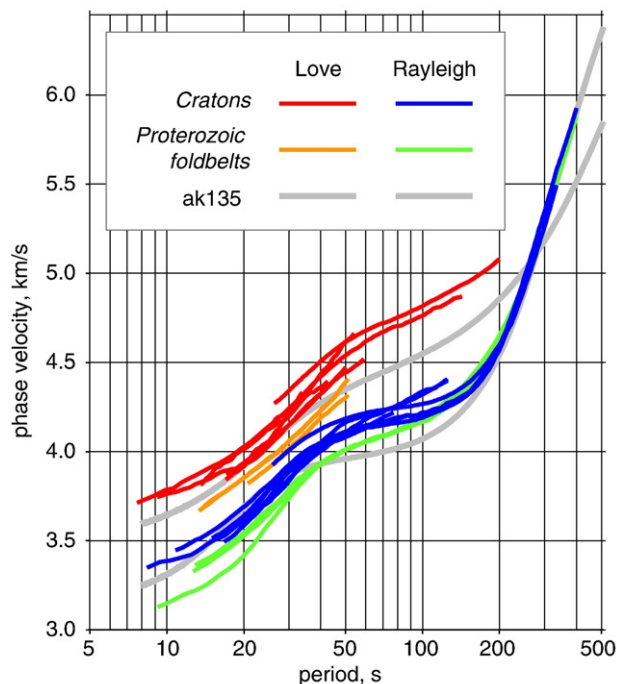


**Fig. 2.** Ten Rayleigh-wave and ten Love-wave dispersion curves measured. Uncertainties of the curves are plotted in Figs. 4–8.

the results obtained in this study; this confirms that at least a large part of the Paraná Basin is indeed a craton (Snoko and James, 1997; Heintz et al., 2005).

The one inter-station path in Africa is across the Archean Congo Craton. The path in Western Australia samples primarily the Archean Yilgarn Craton; its northern portion also traverses the Archean Pilbara Craton and Proterozoic Bangemall Basin.

In Asia, three inter-station paths are across Proterozoic foldbelts, two within the Kazakhstan block and one within the Yangtze Craton. Our data thus sample 7 Archean and Archean–Proterozoic cratons and 3 foldbelts of Proterozoic origin.

### 3. Broad-band phase-velocity measurements

#### 3.1. Method

We measure inter-station surface-wave dispersion using a novel combination of two different techniques (Lebedev et al., 2006). We first measure phase velocities of the fundamental-mode Rayleigh and Love waves by cross-correlating vertical- and transverse-component seismograms, respectively, from the two stations, as implemented by Meier et al. (2004). Cross-correlation produces measurements in broad period ranges, including, in particular, shorter periods (10–20 s). Measurements at these shorter periods are not possible with “source-station” methods that are used to produce large-scale tomographic models. This is because at short periods the observed waveforms are complex, strongly distorted by seismic-wave diffraction. It turns out, however, that the patterns of waveform complexity often change little as seismic waves propagate from one station to another station nearby. Thanks to this, cross-correlation can extract accurate dispersion measurements even from signals that appear prohibitively complex. The (empirical) short-period limit of the measurements varies from station pair to station pair and depends on the distance between the stations and on the lateral heterogeneity within the Earth in the region of the stations. Inter-station distances and period ranges of our measurements are given in Table 1.

We then measure average phase velocities between sources and stations by means of the Automated Multimode Inversion (AMI) of surface- and S-wave forms (Lebedev et al., 2005), and for each pair of successful measurements (same event, both stations) calculate phase velocities between the two stations. Because AMI synthesises complete seismograms, fundamental-mode dispersion can be measured even when the mode interferes with S waves. This is an important advantage for measurements at long periods, because long-period surface waves arrive to stations before intermediate-period ones, often simultaneously with energetic S and multiple S waves, and this makes cross-correlation measurements difficult.

Dispersion curves obtained with the two techniques overlap over most of their frequency bands and are, generally, remarkably consistent (Lebedev et al., 2006). Each of the techniques has advantages over the other, with the cross-correlation, “station-station” technique providing the short-period measurements and the multimode-waveform, “source-station” technique supplying more longest-period measurements, especially for Love waves.

The events that generated the seismograms that we used in this study were selected at back azimuths within  $10^\circ$  from the station-station azimuths. Phase velocities were measured from the phase shifts accumulated over the distance computed as the difference between the distances from the source to each of the two stations of a pair, so that the obvious geometrical effect of a non-zero angle between the station-station and station-event azimuths was taken into account.

Robust inter-station dispersion curves were derived through averaging of tens or hundreds of smooth dispersion curves measured using recordings of different events at the same stations. Cross-correlation measurements can be biased due to the interference of fundamental and higher modes, and both cross-correlation and waveform-inversion measurements can be biased due to surface-wave diffraction (Pedersen, 2006). Because these effects are frequency dependent, they are often manifested in “roughness” of measured curves. Selection of only smooth portions of the curves, removal of outliers (unrealistically far from the average), and subsequent averaging over many measurements—obtained from earthquake signals from different regions and from different directions—combine to enhance the accuracy of the measured dispersion.

The average Rayleigh- and Love-wave phase-velocity curves and their standard deviations were computed from cross-correlation and AMI measurements on signals from tens to hundreds of events. The number of events at suitable azimuths varies from one station pair to another because of the unevenness of the distribution of seismicity over the globe. For our station pair in Africa, only a small number of events could be used (Table 1), especially for Love-wave measurements, and the Love-wave dispersion curve derived is very narrow-band and has large uncertainties. With a larger number of events, the estimated errors (standard deviations) are usually smaller, and the frequency band of accurate measurements can be expected to be broader. The frequency band and errors also depend, however, on lateral heterogeneity, both in the vicinity of the stations and between source regions and the stations (Pedersen, 2006). For the station pair on the Baltic Shield (KEV–LVZ), suitable events are numerous but the estimated uncertainties of the measured dispersion are relatively large (Section 4) because of the scatter in the measurements performed using signal from different events.

#### 3.2. Phase-velocity curves

The results of our measurements are 10 Rayleigh-wave and 10 Love-wave dispersion curves (Fig. 2). Uncertainties of the dispersion curves are shown in the figures in Section 4.

We restricted the period range of each phase-velocity curve so that it included only the most accurate phase-velocity measurements, averaged from many reliable one-event measurements. (The

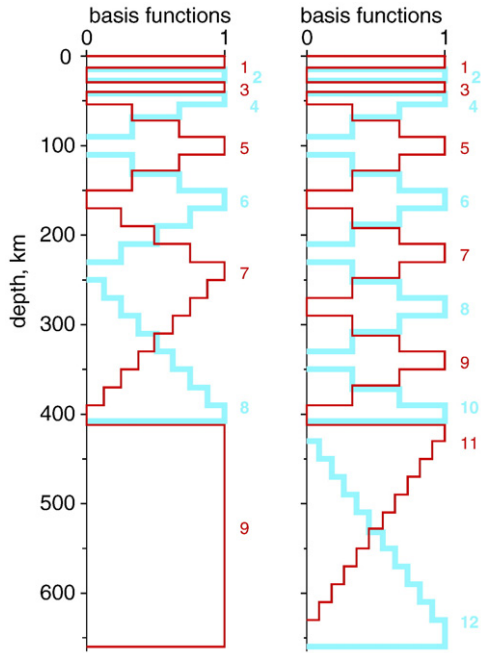


**Fig. 3.** Example sets of 9 (left) and 12 (right) depth basis functions spanning the crystalline crust and upper mantle and used in the inversions of the dispersion data. Line colours and textures are alternated so as to help distinguish neighbouring basis functions. In our inversions of phase-velocity data, each basis function is used to define two independent parameters: one for an isotropic  $V_S$  perturbation and another for the amount of anisotropy within the depth range spanned by the function. Different parameterisations with different numbers of parameters in the mantle, as well as different definitions of damping, were used in series of test inversions for each profile so as to make sure that our results and conclusions are robust with respect to the (arbitrary) choice of the parameterisation. Three more parameters that were used in the inversions were depths to crustal interfaces: the bottom of the upper crust, the bottom of the middle crust, and the Moho. (For interpretation of the references to color in this figure legend, the reader is referred to the web version of this article.)

requirement of many one-event measurements having to be averaged was relaxed (Table 1) for the path in Africa (BGCA–MSKU) and, to a lesser extent, the path across the Paraná Basin (SPB–BDFB) where signal from relatively few events could be used because the inter-station azimuths did not point towards regions of abundant seismicity.) Not all dispersion curves are as broad-band as we would prefer, but the advantage of the conservative data selection is that it gives us confidence in both the phase-velocity values and their estimated errors. Most of the Love-wave curves do not extend to periods over 50 s and thus sample only the crust and upper lithospheric mantle. Rayleigh-wave curves extend to longer periods and sample  $V_S$  structure from the upper crust down to deep upper mantle.

The set of phase-velocity measurements (Fig. 2) displays a number of conspicuous patterns. At periods shorter than 100 s phase velocities are sensitive primarily to  $V_S$  structure in the lithospheric depth range (depths less than 200 km). At these “lithospheric” periods, phase velocities measured on cratons are consistently higher than those measured on Proterozoic foldbelts. From this observation it is apparent that shear velocities  $V_S$  in the lithosphere of the cratons are consistently higher than those in the lithosphere of the younger foldbelts.

Phase velocities at periods 50–150 s are sensitive to  $V_S$  structure mostly in the mantle lithosphere and asthenosphere (down to 250–300 km depth). All measured values in this period range exceed the global averages. (The reference Love and Rayleigh curves were computed for the model AK135 (Kennett et al., 1995) which is slightly faster than global average—closer to continental structure—in its average over the 50–200 depth range.) Mantle lithosphere of all the tectonic units sampled is clearly faster than the global average, in

agreement with the tomographic image in Fig. 1. Crustal structure, including crustal thickness, varies substantially from one location to the other; this is apparent from the broad range of measured values of shorter-period (<30 s) phase velocities that sample primarily the crust.

Seismic heterogeneity in the lower half of the upper mantle—sampled by Rayleigh waves with periods over 200 s—is weaker than in the lithosphere–asthenosphere depth range: phase velocities measured at these periods all plot close to the reference curves.

#### 4. Radially anisotropic shear-velocity profiles

##### 4.1. Inversion

We now use the measured Rayleigh- and Love-wave phase-velocity curves to constrain radially anisotropic  $V_S$  profiles. For each station pair, we invert Rayleigh- and Love-wave dispersion simultaneously for a profile of the average shear speed  $V_S = V_{S(ave)} = (V_{SH} + V_{SV})/2$  and for a profile of the amount of radial anisotropy  $|V_{SH} - V_{SV}|/2$ .  $V_{SH}$  and  $V_{SV}$  are the velocities of horizontally and vertically polarised S waves, respectively, which control phase velocities of Love and Rayleigh waves, respectively. We shall plot (Section 4.2) the Voigt isotropic average  $V_{S(iso)} = (2V_{SV} + V_{SH})/3$  instead of the arithmetic average  $V_{S(ave)}$ ; given the anisotropy we detect, the difference between the two averages is small (less than 1% in the crust and uppermost mantle, less than 0.5% at 100 km and greater depths).

The inversion is performed by means of non-linear optimisation from the MATLAB toolkit. It is not linearised: synthetic Love- and Rayleigh-wave phase velocities are recomputed directly from every perturbed  $V_{SH}$  and  $V_{SV}$  profile, respectively, during the gradient search.

**Table 2**

Isotropic structure of Precambrian lithosphere: station pairs; tectonic units sampled; depth to the Moho  $D_M$  derived from our dispersion data; depth to the Moho  $D_M^{CR2}$  from the global model CRUST2 (Bassin et al., 2000);  $V_S$  gradient in the lithospheric mantle from the Moho down to 100–150 km (“+” for a  $V_S$  increase with depth); ranges of  $V_S$  averages in the mid-lithosphere (100–150 km) consistent with the data;  $V_S$  gradient in the lower lithosphere or below the lithosphere (“–” for a decrease of  $V_S$  with depth, i.e. the presence of a lower-velocity layer beneath the lithosphere)

No.	Stations	Site	$D_M$ , km	$D_M^{CR2}$ , km	$V_S$ gradient below the Moho	$V_S$ at 100–150 km depth, km/s	$V_S$ gradient near the bottom of the lithosphere
<i>Cratons</i>							
1	KEV–LVZ	Baltic Shield	42	42	+	4.62–4.82	–
2	PUL–TRTE	Russian Platform	48	41	+	4.58–4.78	
3	MHV–OBN	Russian Platform	48	47	+	4.63–4.94	
4	PTGA–KOG	Guyana Shield	41	33		4.64–4.76	– – –
5	BDFB–SPB	Paraná Basin	38	39	+	4.62–4.76	– –
6	BGCA–MSKU	Congo Craton	41	39	++		
7	MBWA–NWA0	Western Australia		37	+	4.71–4.86	– – –
<i>Proterozoic foldbelts</i>							
8	BRVK–KURK	Kazakhstan	45	42	+	4.56–4.67	
9	KURK–MAKZ	Kazakhstan	49	45	+	4.49–4.71	
10	ENH–XAN	Yangtze Craton	42	35	+	4.49–4.75	–

“+” (“–”): the increase (decrease) is preferred by the data; “++” (“– –”): the increase (decrease) is strongly preferred by the data; “+ + +” (“– – –”): the increase (decrease) is required by the data. No entry means that this property at this location is either insufficiently constrained or not favoured by the present dispersion data.

Compressional velocity  $V_p$  has a relatively small but not negligible effect on Rayleigh-wave phase velocity; perturbations in  $V_p$  were assumed isotropic and coupled to the perturbations in isotropic-average shear speed as  $\delta V_p$  (m/s)  $\equiv$   $\delta V_s$  (m/s) (the principal results discussed below do not change if different reasonable coupling definitions are assumed). Parameterisation of  $V_s$  models can have a substantial impact on their appearance. We use three boxcar basis functions for the upper, middle, and lower crust, and 6–9 overlapping triangular basis functions in the mantle (Fig. 3), depending on the depth down to which measurements for the station pair constrain  $V_s$  structure. Each basis function in the crust and mantle defines the sensitivity depth range of two independent inversion parameters, one for isotropic-average  $V_s$  and one for the amount of anisotropy. Because short-period measurements are missing for our longest path in Western Australia, in this case we use a single inversion parameter for the upper and middle crust and do not allow anisotropy there.

Our choice of parameterisation was aimed at introducing minimal *a priori* complexity into the models. The judgement on the amount of complexity in a model is somewhat subjective. The choice of the triangular basis functions allows for various gradients in both isotropic and anisotropic structure but not for sharp discontinuities between the Moho and the 410 km depth.

The reference models in the initial inversions comprised the structure in the mantle from the 1D reference model AK135 and structure in the crust from the 3-D global crustal model CRUST2 (Bassin et al., 2000). The reference crustal profile for each station pair was computed as an average over CRUST2 structure along the inter-

station path. In subsequent inversions, reference models were updated and included best-fitting crustal structure according to previous inversions and mantle profiles with  $V_s$  that was faster than AK135 and constant from the Moho down to a 250–350 km depth, below which the profile continued as AK135.

In addition to  $V_s$  and anisotropy, we also invert for the depths of three discontinuities, those at the bottom of the upper, middle, and lower crust. The latter (the Moho) is constrained best. It is important to use a reasonably accurate reference value for the Moho depth and to let the depth vary in the inversion because it can trade-off both with isotropic structure in the crust and uppermost mantle and with radial anisotropy (Levshin and Ratnikova, 1984). Our estimates of the Moho depth beneath each of the 10 locations are given in Table 2, along with those from CRUST2. Although a wide range of Moho depths can be consistent with observed surface-wave dispersion within errors, best-fitting values obtained in inversions of broad-band data such as in this study turn out to be fairly accurate estimates, closely matching receiver-function results where those are available (e.g. Endrun et al., 2004; Lebedev et al., 2006).

#### 4.2. Preferred S-velocity profiles

We perform two sets of inversions. One includes inversions for “preferred” profiles beneath each of the 10 locations; these profiles provide a close fit to the data. The other is an extensive series of (hundreds of) tests designed to explore the model spaces of the inverse problems so as to infer the presence or absence of  $V_s$  gradients

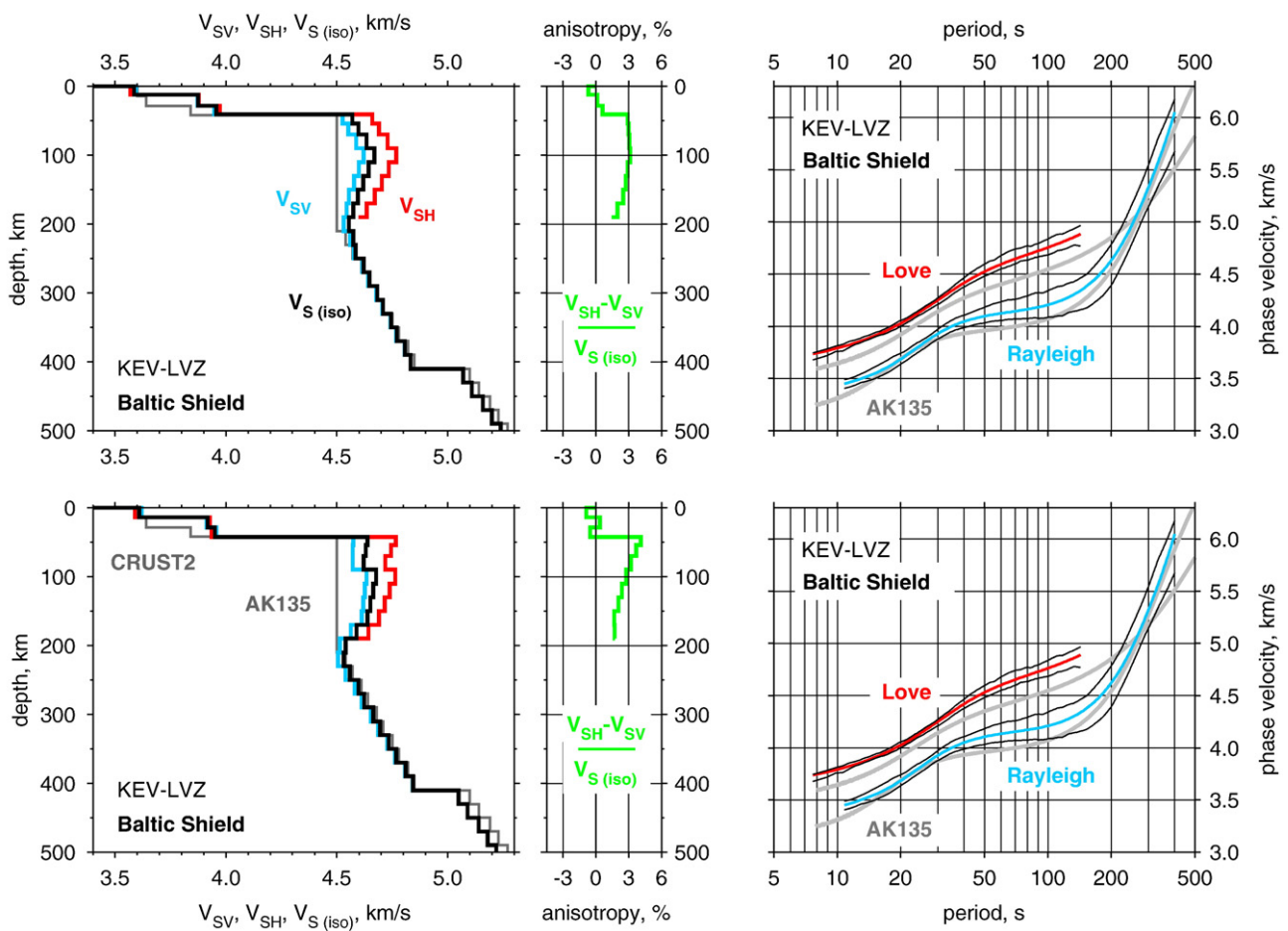


**Fig. 4.** Two radially anisotropic S-velocity profiles that fit the data from the Baltic Shield. Left: the profiles of  $V_{SV}$ ,  $V_{SH}$ , the isotropic average  $V_s$  ( $V_{S(iso)} = (2V_{SV} + V_{SH})/3$ ), and radial anisotropy are plotted in the depth range in which they are constrained by the data. Right: synthetic Love- and Rayleigh-wave dispersion curves computed for the  $V_{SH}$  and  $V_{SV}$  profiles, respectively, and the measured phase velocities plus/minus the error bars (thin black lines).

and radial anisotropy at different depths and to map ranges of  $V_S$  values that are consistent with the data.

Our preferred models (Figs. 4–8) are computed with mild damping on isotropic anomalies and on the amount of radial anisotropy. As any models yielded by inversions of data with finite errors, they are non-unique. In Fig. 4 we show two different models for the Baltic Shield, both fitting the data well. The data (slightly) favours that  $V_S$  in the depth range from the Moho to ~100 km is lower than in the 100–150 km depth range. This increase in  $V_S$ , however, can be modelled both with a positive  $V_S$  gradient below the Moho (Fig. 4, top) and with a discontinuity, for example at a 90 km depth (Fig. 4, bottom).

We attribute the increase in  $V_S$  between the Moho and ~100 km depth to the occurrence of the transition from spinel peridotite to garnet peridotite (Hales, 1969). Introducing a discontinuity at 90 km (Fig. 4, bottom), we can fit the data with a profile that, at the same time, features decreases in  $V_S$  with depth both above and below 90 km, as would be expected given the increase in temperature with depth. Our data, however, cannot constrain the depth or the sharpness of this discontinuity. And the spinel–garnet transition may in fact occur over a depth interval tens of kilometers wide (Klemme, 2004), which would produce a  $V_S$  gradient rather than a discontinuity, bringing us back towards the profile in Fig. 4 (top). The introduction of such a discontinuity *a priori* thus brings into the model a complexity that is not particularly favoured either by our measurements or by mineralogical data. We, therefore, choose to parameterise the inversions for the preferred profiles so as to allow only smooth gradients between the Moho and 410 km depth.

Overviewing the 10 preferred  $V_S$  models (Figs. 4–8), we observe the Proterozoic foldbelt lithosphere to be seismically faster than the global average but slower than the lithosphere beneath cratons. Cratonic mantle lithosphere is, as expected, much faster than average.

An increase in  $V_S$  between the Moho and a 100–150 km depth appears in all the profiles. A  $V_S$  decrease around a 200 km depth—near the bottom of the seismic lithosphere—is seen in most but not all profiles, and its magnitude is clearly different in different locations.

Radial anisotropy indicative of horizontal fabric in the lower crust and upper mantle lithosphere ( $V_{SH} > V_{SV}$ ) is preferred by the data in most Precambrian locations sampled. In the upper crust, radial anisotropy, where detected, is with  $V_{SH} < V_{SV}$ , indicating vertical fabric.

#### 4.3. Exploring the model spaces

$V_S$  profiles such as in Figs. 4–8 are non-unique solutions of inverse problems. Can we distinguish robust properties of the lithospheric models from “accidental” features that are not required or even particularly favoured by the data? Attaching error-bar estimates to the profiles would not necessarily help in the interpretation because they would give no information on the trade-offs between anomalies at different depths and between isotropic and anisotropic structure. Monte-Carlo-type inversions are effective in exploring complete model spaces, i.e. mapping ranges of models compatible with the data (e.g. Shapiro and Ritzwoller, 2002; Endrun et al., 2008), but the interpretation of the resulting broad ranges of values is also not

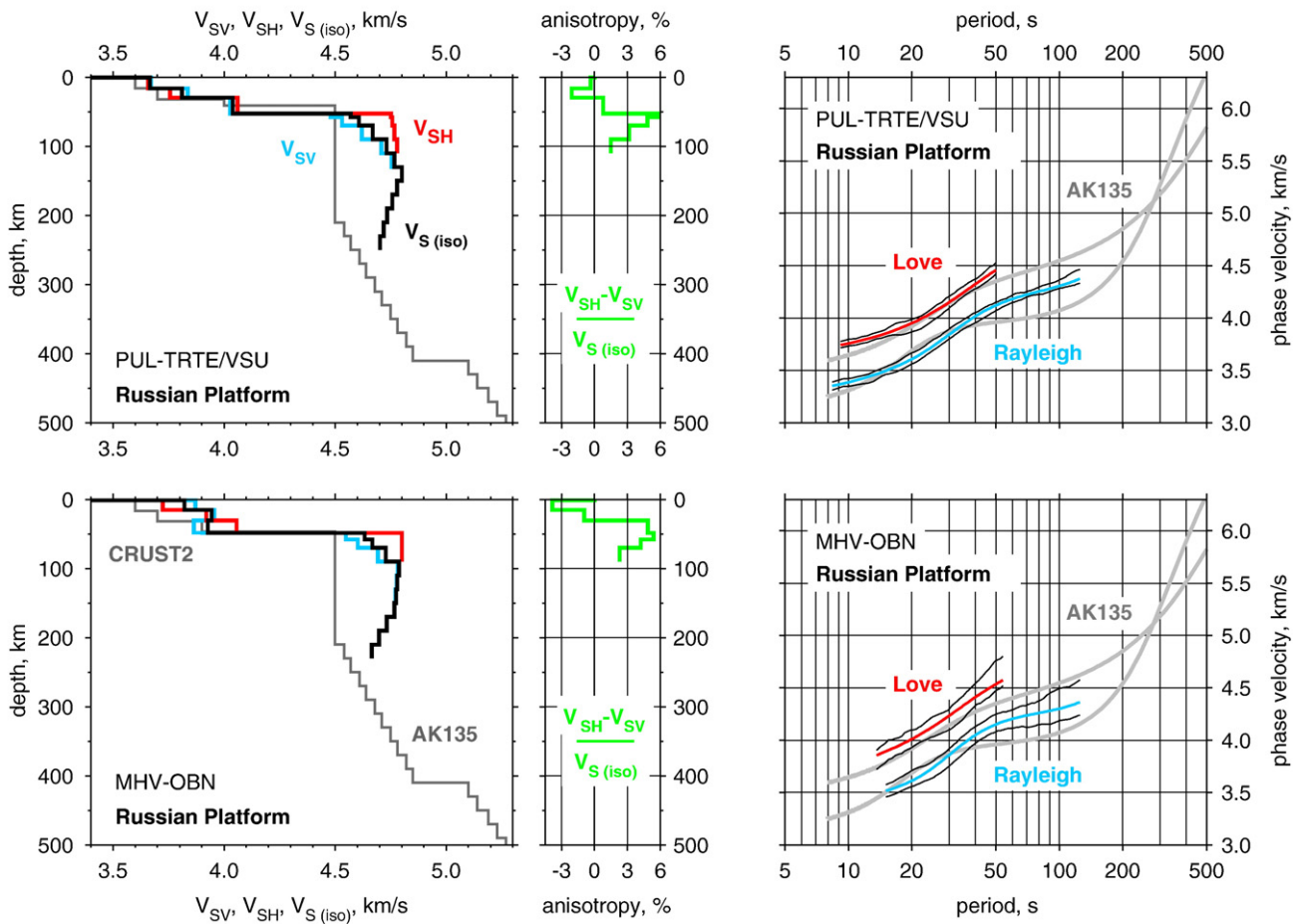
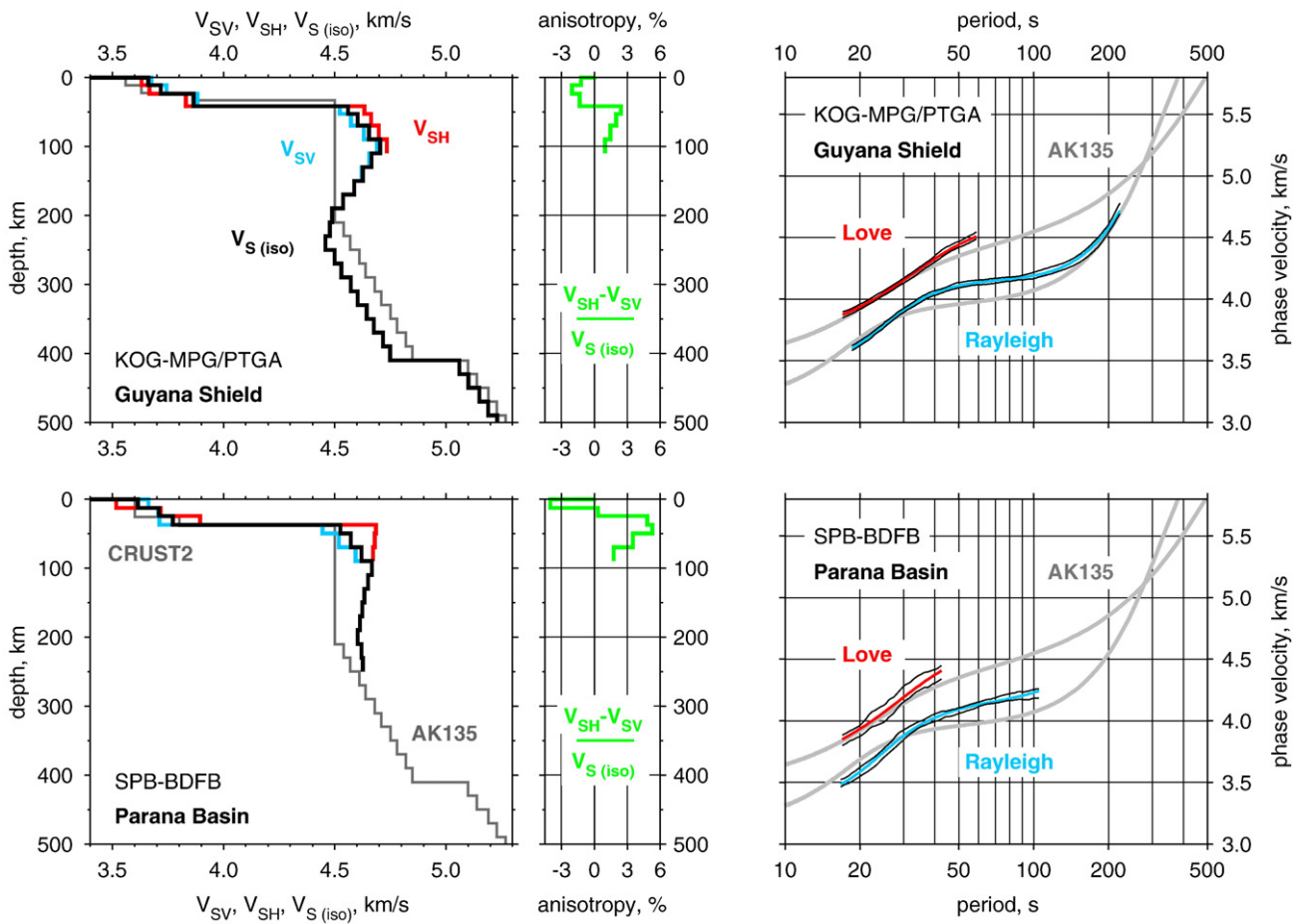


Fig. 5. Preferred radially anisotropic S-velocity profiles for two locations on the Russian Platform (Table 1; Fig. 1). Left: the profiles of  $V_{SV}$ ,  $V_{SH}$ , the isotropic average  $V_S$  ( $V_{S(iso)} = (2V_{SV} + V_{SH})/3$ ), and radial anisotropy are plotted in the depth range in which they are constrained by the data. Right: synthetic Love- and Rayleigh-wave dispersion curves computed for the  $V_{SH}$  and  $V_{SV}$  profiles, respectively, and the measured phase velocities plus/minus the error bars (thin black lines).



**Fig. 6.** Preferred radially anisotropic S-velocity profiles for two locations in South America, the Guyana Shield and the Paraná Basin (Table 1; Fig. 1). Left: the profiles of  $V_{SV}$ ,  $V_{SH}$ , the isotropic average  $V_S$  ( $V_{S(iso)} = (2V_{SV} + V_{SH})/3$ ), and radial anisotropy are plotted in the depth range in which they are constrained by the data. Right: synthetic Love- and Rayleigh-wave dispersion curves computed for the  $V_{SH}$  and  $V_{SV}$  profiles, respectively, and the measured phase velocities plus/minus the error bars (thin black lines).

straightforward in the presence of the trade-offs. The Neighbourhood Algorithm (Sambridge, 1999a,b)—applied in its entirety to a global phase-velocity data set—enabled Beghein and Trampert (2003, 2004) to explore model spaces while targeting the probabilities of particular properties of the models and to derive robust constraints on average radial anisotropy in different depth intervals beneath continents and oceans of different age.

In this study we take advantage of the small size of our inverse problems and of the relative simplicity of the associated model spaces and employ a different approach of model-space exploration, simple but effective. We identify seismic properties that we wish to constrain and for each of them run a series of targeted test inversions.

In order to determine the range of the  $V_S$  average over 100–150 km depths within the mantle lithosphere, we parameterise the lithosphere so that  $V_S$  is constant between 90 and 150 km depths and increases by 0.14 km/s from the Moho to 90 km depth (such an increase is suggested by our preferred profiles). Assuming a value of  $V_S$  at 90–150 km and letting the structure in the crust and below 150 km vary freely, we run a gradient search and find a  $V_S$  profile that fits the data best. If the dispersion curves computed for this profile fall within error bars of the measured curves, then we conclude that this value of  $V_S$  at 90–150 km is consistent with the data. In Fig. 9 we show the fastest and the slowest models of the lithosphere beneath Western Australia that are consistent with our measurements. The synthetic phase-velocity curves are at the limits given by the error bars of the measurements: lithospheric  $V_S$  that is 0.01 km/s slower than in the slowest model (top) or 0.01 km/s faster than in the fastest

model (bottom) would force synthetic dispersion curves outside the error bars and would thus not fit the data. We estimate that these fastest and slowest models limit the range of  $V_S$  values at 100–150 km depth that are consistent with our measurements. The *a priori* choice of the  $V_S$  gradient in the Moho–90 km depth range has a simple effect: a smaller gradient would shift the inferred limits of the  $V_S$  range (especially the upper limit) slightly down; a higher gradient would shift the inferred limits of the  $V_S$  range (especially the lower limit) slightly up. Overall, our mapping of the  $V_S$  range is conservative: the shapes of the synthetic dispersion curves computed for the slowest and fastest profiles are strongly distorted compared to measured curves but are still considered acceptable.

Other properties we wish to constrain are  $V_S$  gradients and radial anisotropy at different depths. Taking the same approach as for mapping  $V_S$  ranges, we found that most gradients seen in the preferred profiles are not required by the data: if bent sufficiently, synthetic dispersion curves for models without the gradients fit the measurements within the error bars. This approach, however, appears to be much too conservative: if a feature is clearly favoured by the data (provides better fit) at most of the locations we sample then it is probable that the feature is indeed present in the Earth.

We, then, distinguish three degrees of how much a lithospheric property is favoured by the measurements: the property is “preferred” if the data is fit better with it present than with it absent; “strongly preferred” if without it the models are only marginally consistent with the data (like models in Fig. 9); “required” if we could not find any models without this property that fit the data within errors.

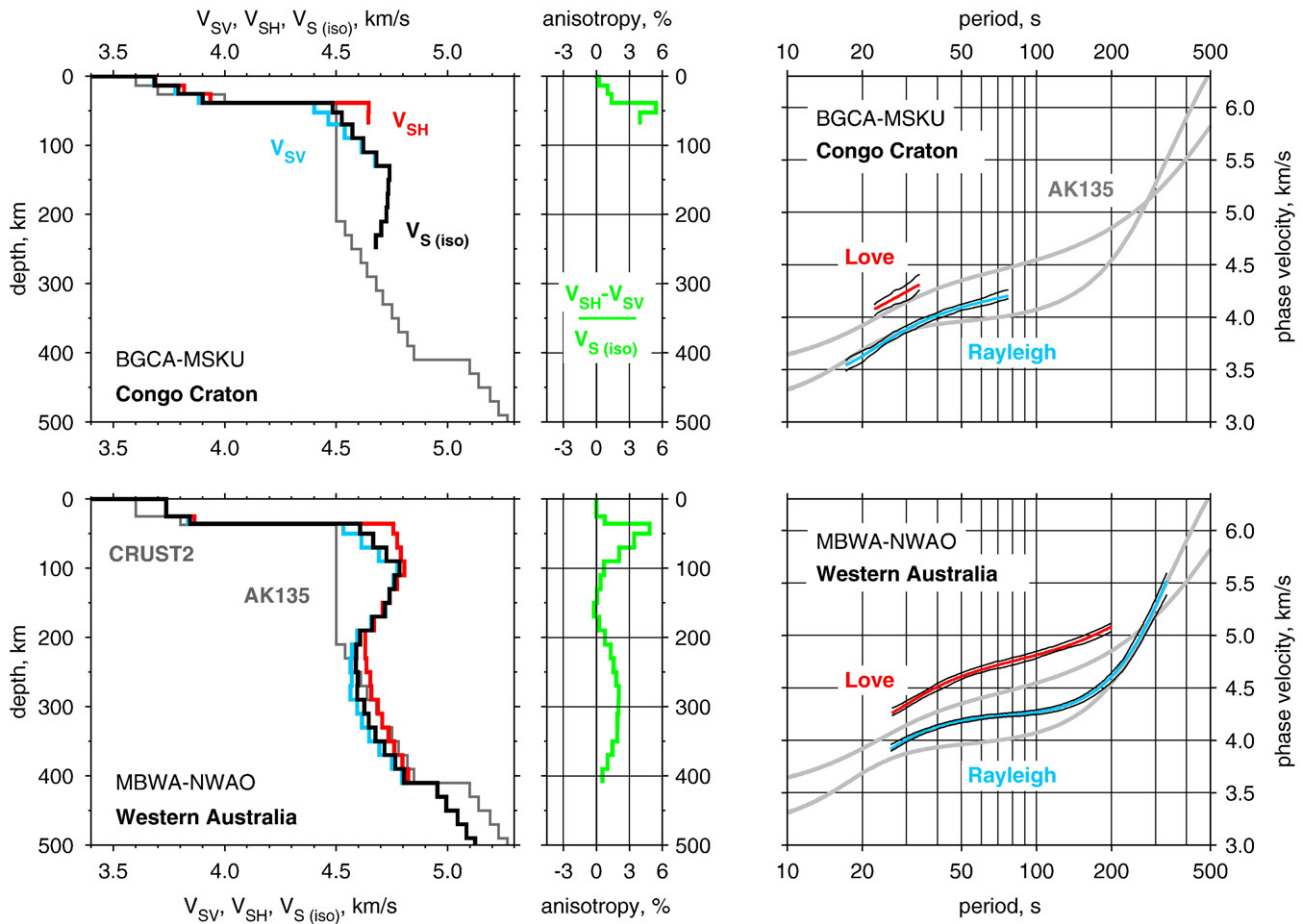


**Fig. 7.** Preferred radially anisotropic S-velocity profiles for the Congo Craton and Western Australia (Table 1; Fig. 1). Left: the profiles of  $V_{SV}$ ,  $V_{SH}$ , the isotropic average  $V_S$  ( $V_{S(iso)} = (2V_{SV} + V_{SH}) / 3$ ), and radial anisotropy are plotted in the depth range in which they are constrained by the data. Right: synthetic Love- and Rayleigh-wave dispersion curves computed for the  $V_{SH}$  and  $V_{SV}$  profiles, respectively, and the measured phase velocities plus/minus the error bars (thin black lines).

The results of the extensive series of test inversions—dozens of inversions for each station pair, with different reference models and different parameterisations and regularisations—are summarised in Tables 2 and 3.

The increase in  $V_S$  between the Moho and a 100–150 km depth is preferred (as denoted by +, ++ in Table 2) by almost all our measurements (the data can be fit within uncertainties without this increase but the fit is better with it than without it).

Among the  $V_S$  ranges at 100–150 km depth that are consistent with the data, some are broader than others, mainly because of larger measurement uncertainties (e.g. MHV–OBN). The most likely (best-fitting)  $V_S$  values are close to the middle of the ranges.

Shear-wave speed at 100–150 km depth appears to be different beneath the different cratons sampled. The average over all 6 cratonic locations (with the worst-sampled Congo Craton excluded) is 4.73 km/s. This is 5% higher than AK135 and ~6% higher than the global average according to the model of Lebedev and van der Hilst (2008). This value would, also, fit the data within uncertainties for each of the cratons sampled (Table 2).

Beneath Proterozoic foldbelts,  $V_S$  at 100–150 km depth is lower than beneath cratons. The average over the three foldbelts is 4.61 km/s, ~2% faster than AK135 and ~3% faster than the global average (Lebedev and van der Hilst, 2008).

A decrease in  $V_S$  below 150–200 km is preferred or required by the data only in half of the locations (as denoted by -, --, --- in Table 2). Beneath the rest of the locations, the data can be fit equally well with and without such a decrease. Beneath Guyana shield, there is a

pronounced low-velocity zone and the data requires that  $V_S$  beneath the lithosphere is lower than the global average.

Radial anisotropy with  $V_{SH} > V_{SV}$  (horizontal fabric) is preferred (+, ++) in both the lower crust and the lithospheric mantle beneath most of the locations (Table 3). Retrieved anisotropy in the lithospheric mantle can trade off with that in the lower crust: some of our measurements can be matched by models with anisotropy either in the lower crust only or in the lithospheric mantle only. We thus examine the presence of anisotropy over the entire lower-crust–lithospheric-mantle depth range. Over this depth range, anisotropy with  $V_{SH} > V_{SV}$  is either strongly preferred or required (++, +++) at almost all locations.

Anisotropy in the lower lithosphere (below ~100 km) is unconstrained by the measurements at most of the locations because of the lack of long-period Love-wave measurements.  $V_S$  distributions below 100 km depth at those locations are derived assuming  $V_{S(iso)} \approx V_{SV}$ . Where sampled by the data, radial anisotropy in the lower lithosphere (100–200 km depths) appears to be either rather weak (Fig. 4) or absent (Fig. 7).

Radial anisotropy in the upper crust is required in one location (---) and preferred by the data in three others (-); it is consistently with  $V_{SH} < V_{SV}$ , indicating vertical fabric (Table 3).

## 5. Discussion

We assume that any one of the dispersion curves we have measured may be somewhat biased due to undetected diffraction effects. We also assume that substantial azimuthal anisotropy may be

common within cratonic lithosphere (e.g. Fouch and Rondenay, 2006; Deschamps et al., 2008a) and, even though radial anisotropy probably occurs in addition to azimuthal anisotropy (Gaherty and Jordan, 1995), and the azimuthal anisotropy signal in Love and Rayleigh data may average out to some extent over the length of an inter-station path, we assume that any of our radially anisotropic profiles can be biased due to the mapping of the (unknown) azimuthal anisotropy into radial anisotropy. Isotropic heterogeneity can also map into radial anisotropy models (Levshin and Ratnikova, 1984). We therefore focus our interpretation on the most basic features of the profiles and on persistent patterns that are detected repeatedly.

5.1. Lithospheric  $V_S$  increase with depth: “Hales gradient”?

An increase in  $V_S$  between the Moho and a 100–150 km depth has featured—either as a gradient or as a discontinuity—in numerous seismic models of continents (e.g. Paulssen, 1987; Gaherty and Jordan, 1995; Ekström, 2000; Freybourger et al., 2001; Lebedev and Nolet, 2003; Bruneton et al., 2004; Fishwick et al., 2005; Levshin et al., 2007). Such an increase cannot be explained by a change in temperature with depth (Faul and Jackson, 2005). Shapiro and Ritzwoller (2004) argued that they can fit global group- and phase-velocity maps within estimated errors with  $V_S$  profiles featuring no increase but, instead, a

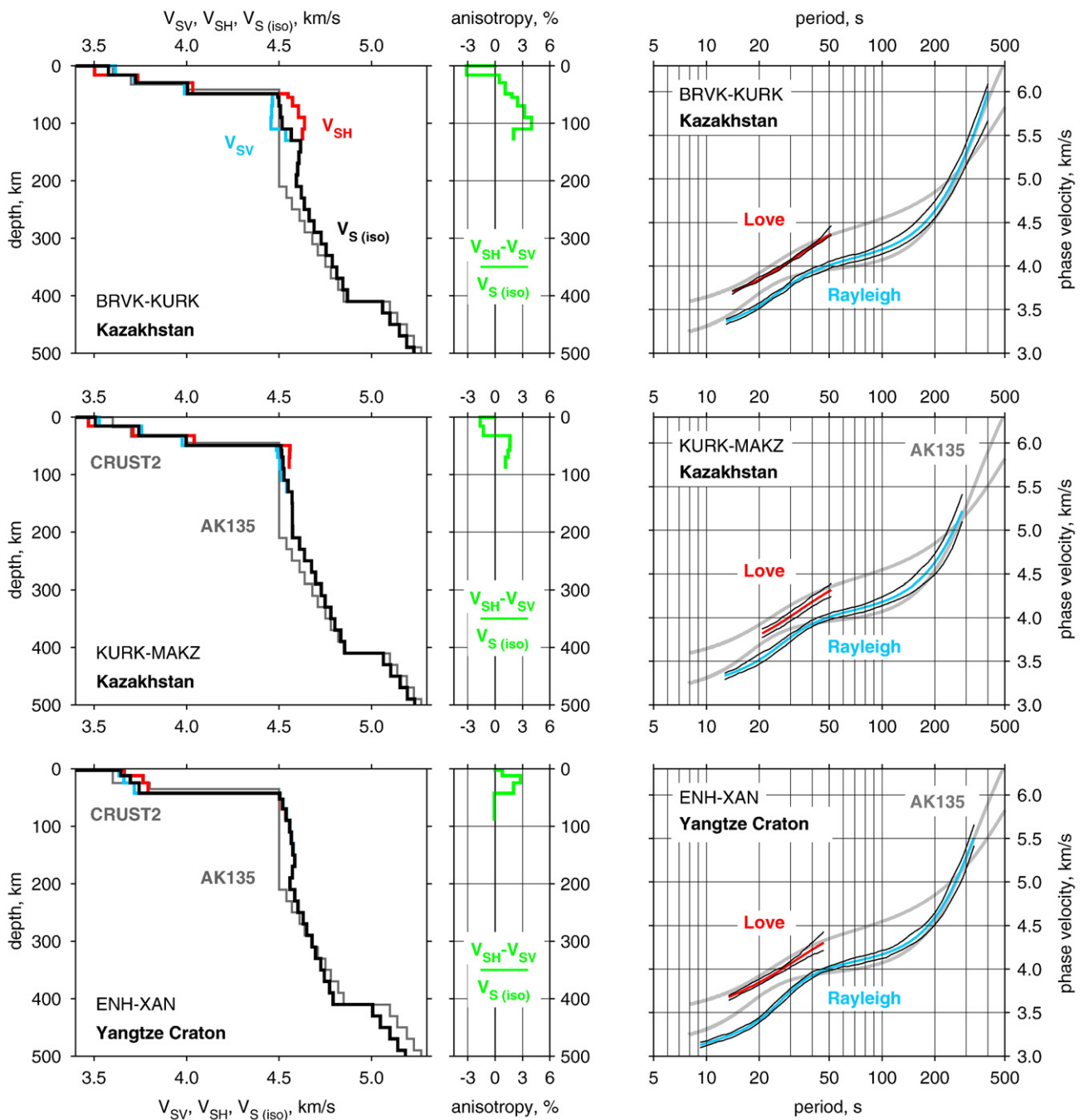


**Fig. 8.** Preferred radially anisotropic S-velocity profiles for three Proterozoic foldbelts in Asia (Table 1; Fig. 1). Left: the profiles of  $V_{SV}$ ,  $V_{SH}$ , the isotropic average  $V_S (V_{S(iso)} (2V_{SV} + V_{SH})/3)$ , and radial anisotropy are plotted in the depth range in which they are constrained by the data. Right: synthetic Love- and Rayleigh-wave dispersion curves computed for the  $V_{SH}$  and  $V_{SV}$  profiles, respectively, and the measured phase velocities plus/minus the error bars (thin black lines).

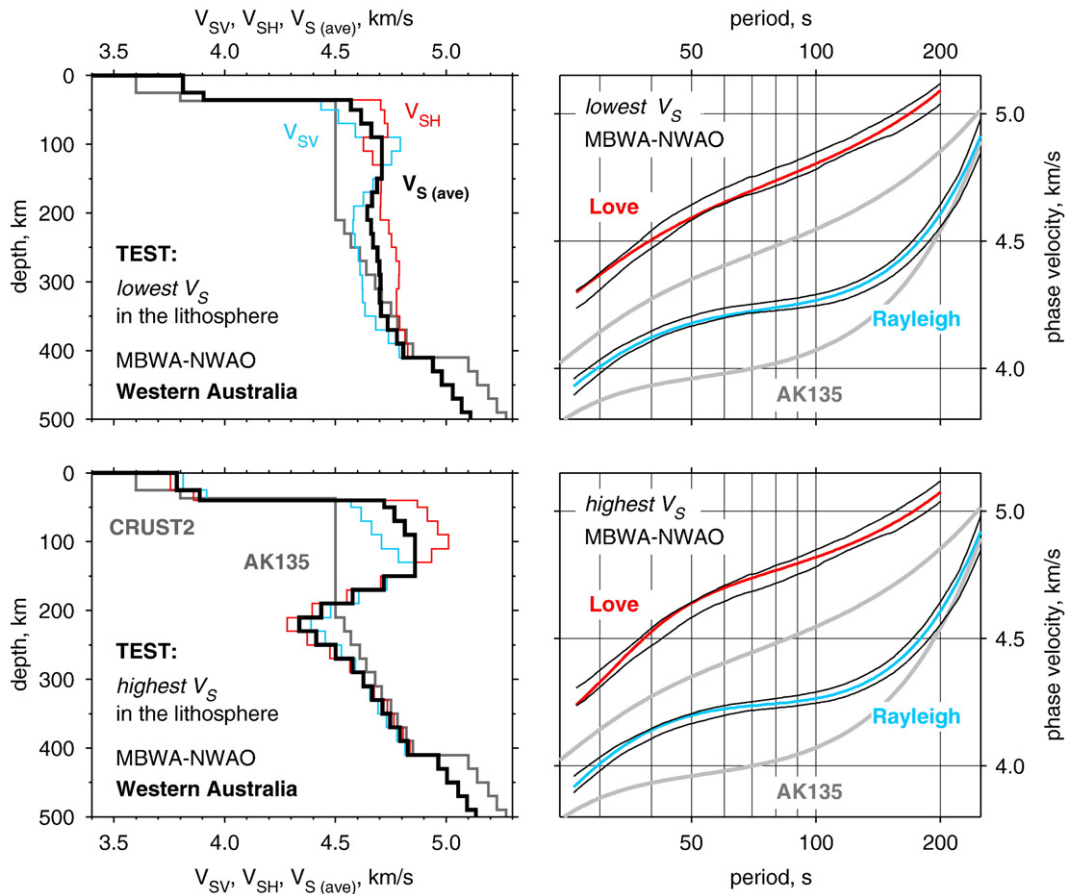


**Fig. 9.** Two tests from a test series performed to delimit the range of  $V_S$  in the lithosphere of Western Australia that is consistent with the data. Left: the profiles of  $V_{SV}$ ,  $V_{SH}$  and the average  $V_S$ . Right: synthetic Love- and Rayleigh-wave dispersion curves computed for the  $V_{SH}$  and  $V_{SV}$  profiles, respectively, and the measured phase velocities plus/minus the error bars (thin black lines). Top: the model with the lowest lithospheric  $V_S$  consistent with the data; if  $V_S$  in the 100–150 km depth range is 0.01 km/s lower than in this profile, the synthetic dispersion curves do not fit the data within error bars. Bottom: the model with the highest lithospheric  $V_S$  consistent with the data; if  $V_S$  in the 100–150 km depth range is 0.01 km/s higher, the synthetic dispersion curves do not fit the data.

monotonic decrease in  $V_S$  below the Moho and suggested that such models should be preferred as physically plausible.

Although our dispersion measurements do not strictly require an increase in  $V_S$  with depth in the uppermost mantle, this feature is favoured by the data in almost all of the sampled locations (Table 2). This suggests a high likelihood of the presence of this increase within Precambrian lithosphere.

Hales (1969) proposed a discontinuity at a depth of 80–90 km in order to explain regional travel time observations in the Lake Superior region and attributed the discontinuity to the transformation from spinel peridotite to garnet peridotite. Revenaugh and Jordan (1991) found evidence for this discontinuity in ScS reverberation data and estimated the increase in  $V_S$  at this interface at 3.8%. Both a sharp discontinuity and a relatively thick gradient zone (~30 km or thicker if the gradient has a steeper onset) would probably account equally well for the observed reflections of long-period S waves.

The  $V_S$  profile computed by Stixrude and Lithgow-Bertelloni (2005) for a pyrolytic bulk composition and a continental geotherm featured a major “garnet in” jump near a 50 km depth; the depth of the jump was underestimated because the  $Cr_2O_3$  component was not considered (MacGregor, 1970; Stixrude and Lithgow-Bertelloni, 2005). Klemme (2004) showed that the addition of chromium would not only shift the phase transition to higher pressures (greater depths in the Earth) but also make it spread over a broad depth interval. The width of the spinel–garnet coexistence interval (seismic gradient zone in the upper mantle) would increase with increasing  $Cr/(Cr+Al)$  ratio and could be tens of kilometers or even greater.

Analysing xenoliths from alkali basalts and kimberlites, Grütter et al. (2006) found low bulk ratios  $Cr/(Cr+Al) < 0.2$  in lherzolitic xenoliths from alkali basalts but high  $Cr/(Cr+Al)$  in xenoliths from kimberlites: ~0.35 and ~0.45 in chromite-saturated lherzolite and Ca-free harzburgite, respectively. The high  $Cr/(Cr+Al)$  values in the samples from kimberlites imply that the spinel peridotite–garnet peridotite transformation beneath cratons may occur over a broad depth interval, with spinel and garnet co-existing down to below 100 km (Klemme, 2004; Grütter et al., 2006). Studying xenoliths from the Slave Craton, Kopylova and Caro (2004) mapped spinel peridotite compositions down to ~100 km depth and co-existing spinel and garnet down to as far as ~140 km depth, confirming that the spinel–garnet transition beneath cratons may indeed be both deep and broad.

The transformation from spinel peridotite to garnet peridotite could thus account for at least a large part of the increase in  $V_S$  with depth within the upper ~100 km of the mantle. Recently, Bruneton et al. (2004) argued that such a  $V_S$  increase—identified by them in the central Baltic Shield—could be due to chemical layering, with clinopyroxene-rich melting residues decreasing the bulk seismic velocities in the upper part of the lithospheric mantle. Such layering would be consistent with our observations as well. The spinel–garnet transition, however, appears to provide a much simpler explanation for the apparently ubiquitous  $V_S$  increase within the top ~100 km of the mantle. The phase transformation must occur globally and it is expected to cause substantial increases in bulk seismic velocities (Stixrude and Lithgow-Bertelloni, 2005), the increases probably being

over broader depth intervals beneath cratons than elsewhere (Grütter et al., 2006). We argue that the spinel–garnet transition is likely to be the primary cause of the observed gradients, even though compositional heterogeneity—where present—will also play a role in shaping seismic-velocity profiles (Bruneton et al., 2004; Fishwick and Reading, 2008).

The data of Hales (1969) and Revenaugh and Jordan (1991) suggest the presence of a relatively sharp  $V_S$  increase, but this can be brought about both by a sharp discontinuity and by a steeper onset of a gradient extending over tens of kilometers. With surface-wave data we also cannot determine the sharpness of the transition. Thus, either a Hales discontinuity or a “Hales gradient”—both possibilities consistent with seismic data—may describe the  $V_S$  increase with depth in the uppermost mantle.

In a paper in this volume, Pedersen et al. (2009–this issue) argue that the Cr content in cratonic lithosphere could be low, so that the spinel–garnet transition may occur at depths too shallow to fully account for the slower-than-expected, lithosphere-sampling parts of their dispersion curves measured on cratons; they review a number of explanations that are alternative to the spinel–garnet transition. Different observations from different cratons thus lead Pedersen et al. (2009–this issue) and us to a similar conclusion, that  $V_S$  in the uppermost mantle is lower than it would be if the mantle rock had the same physical properties at different depths within the lithosphere. In other words, the  $V_S$  profile in the upper mantle lithosphere is not shaped by the temperature distribution only. Disagreements remain over the explanation for this; further work on the properties of the spinel–garnet transition as well as on chemical composition and seismic structure of cratonic lithosphere should help us to establish the roles of the phase transformation and other factors with more certainty.

### 5.2. $V_S$ and temperature within the lithosphere

Beneath the cratons sampled, lithospheric  $V_S$  at 100–150 km depths is on average about 5% higher than in the reference model AK135. Beneath Proterozoic foldbelts sampled  $V_S$  is 2% higher than in AK135. With respect to the global average of the upper-mantle  $V_S$  model of Lebedev and van der Hilst (2008), the anomalies are about 6% and 3%, respectively.

With cratonic lithosphere ~3% faster, on average, than that of the Proterozoic foldbelts, and with compositional differences probably accounting for less than 1% in this difference (e.g. Deschamps et al., 2002; Schutt and Leshner, 2006), cratonic lithosphere must be substantially colder and, assuming nearly conductive geotherms within the lithosphere, substantially thicker (Priestley and McKenzie, 2006). This is consistent with lithospheric temperature estimates provided by xenoliths and xenocrysts (O'Reilly and Griffin, 2006) and implies that the thermal lithosphere cannot grow as thick beneath Proterozoic foldbelts as it has beneath cratons. This, in turn, points to the presence of a thick, durable, buoyant chemical boundary layer beneath cratons that is absent or is thinner beneath the Proterozoic foldbelts (e.g. Jordan, 1988; Forte and Perry, 2000; Deschamps et al., 2002; Griffin et al., 2003; Lee et al., 2005).

### 5.3. Lithospheric thickness and sub-lithospheric low-velocity zones

A modest low-velocity zone (LVZ) beneath continents can probably result from a normal increase of temperature with depth through solid-state mechanisms (no partial melting) (Stixrude and Lithgow-Bertelloni, 2005; Faul and Jackson, 2005; Kuskov et al., 2006). A decrease in  $V_S$  at 150–250 km—at least a small one—is consistent with our data from all the locations, although beneath half of the locations the data can be fit equally well with and without such a decrease. Beneath some of the cratons, a strong  $V_S$  decrease at 150–250 km is required (Figs. 4–8; Table 2).

Beneath Western Australia, a strong negative  $V_S$  gradient near 150–200 km is required by the data. We also observe low  $V_S$  from ~300 km down to the mantle transition zone (410–660 km depth), 1.5–2% below the global average (Lebedev and van der Hilst, 2008) and ~3% low with respect to AK135. Chevrot et al. (1999) computed receiver functions at the station NWA0 in Southwestern Australia and measured anomalously small differential travel times between arrivals of the waves converted from  $P$  to  $S$  at the 410- and 660-km discontinuities, indicative of an anomalously thin mantle transition zone. Given the Clapeyron slopes of the phase transformations in olivine structure that give rise to the 410- and 660-km discontinuities, thin transition zone indicates high temperature, as confirmed by the correlation between the shear-speed structure and thickness of the transition zone globally (Flanagan and Shearer, 1998; Lebedev et al., 2003) and, more specifically, in the Australia–East Asia region (Lebedev et al., 2002).

Both our present measurements and receiver-function evidence suggest that sub-lithospheric mantle beneath Western Australia is warmer than average. The temperature in the lithosphere, however, is as low as beneath any of the cratons, according to the high lithospheric  $V_S$  (Fig. 7; Table 2). It follows either that the Western Australia lithosphere is thicker than that of the other cratons, or that the upper-mantle geotherm beneath Australia is not in equilibrium: relatively cold (in cratonic terms) lithosphere is underlain by a relatively hot mantle below. The Australian continent has been moving over underlying mantle rapidly (current rate ~8 cm/year (Gripp and Gordon, 1990; Argus and Gordon, 1991)). If only the top 200–300 km of the mantle move coherently with the craton, then the cold Western Australia lithosphere has moved atop a hot mantle region that is currently below it only recently; this would account for a non-equilibrium geotherm.

Beneath Guyana Shield, there is a pronounced LVZ and the data requires that  $V_S$  beneath the lithosphere is lower than the global average. An unusual, prominent LVZ beneath this craton has been seen in recent tomographic models (Heintz et al., 2005; Lebedev and van der Hilst, 2008). Lebedev and van der Hilst (2008) proposed that the broad LVZ beneath central and northern South America is a seismic image of hot material, possibly of plume origin, trapped (“ponded”) beneath the thick cratonic lithosphere, as suggested by Sleep (2003) in order to explain hotspot-like volcanism near South America's eastern shores.

The lithosphere of Guyana Shield is thick and cold (although, apparently, not quite as cold as beneath Western Australia), according to the observation of high  $V_S$  within it. If the Guyana Shield lithosphere is as thick as that of Western Australia, then a sub-lithospheric thermal anomaly would decrease the temperature at 100–150 km only modestly (even assuming an already equilibrated geotherm). This decrease would be smaller than the difference in lithospheric temperature due to a difference in the thickness of the lithosphere (thermal boundary layer), such as between cratons and younger continents.

O'Reilly and Griffin (2006) estimate the thickness of the buoyant, basalt-depleted compositional lithosphere beneath cratons and Proterozoic locations at 160–250 and 140–180 km, respectively. From our data, we can estimate the thickness of the seismic lithosphere when there is an LVZ beneath it. For Guyana Shield—underlain by an unusually prominent LVZ—we performed a series of test inversions and found that the best-fitting values for the top of the LVZ are in the 190–250 km depth range. Because  $V_S$  values that we find within cratonic lithospheres are similar, we can assume that the lithospheric thicknesses of the cratons are also similar (Priestley and McKenzie, 2006), and infer that cratonic lithospheres normally bottom in the 190–250 km depth range. The thicknesses of the seismic and compositional lithospheres of cratons thus appear to match closely. There are no LVZs beneath the Proterozoic locations that we sampled; we can only infer from the lower lithospheric  $V_S$  that the stable lithosphere there is likely to be thinner.

#### 5.4. Fabric and anisotropy in the upper crust

Radial anisotropy in the upper crust is required or preferred by the data in four Archean and Proterozoic locations we sampled. The anisotropy is consistently with  $V_{SH} < V_{SV}$  (Table 3).

This radial anisotropy is likely to be due to vertically oriented anisotropic fabric in the upper crust. An alternative possibility that has to be considered is the effect of cracks. Azimuthal anisotropy in the upper crust can be caused by oriented cracks and micro-fractures (e.g. Meissner et al., 2006), opening due to tectonic stress. Radial anisotropy—or apparent radial anisotropy (a projection of azimuthal anisotropy on the direction of the inter-station path that would depend on the orientation of the inter-station azimuth relative to the azimuths of the maximum compression and extension)—could also be attributed to cracks. However, because current deformation within the stable tectonic blocks sampled in this study is small, and because the azimuths of inter-station paths for which we detect anisotropy appear to be at various angles to the azimuths of the maximum horizontal compressive stress at the locations (Reinecker et al., 2005), we conclude that the radial anisotropy observed is due to anisotropic fabric in the crustal rocks, frozen since the time of the last major tectonic episodes.

Archean and Paleoproterozoic orogens differ structurally from contemporary ones, which suggests that the deformation style in Archean/Paleoproterozoic may have been different (Marshak, 1999). Field observations in Archean and Paleoproterozoic transpressive belts yielded evidence for large strains with strong sub-vertical stretch, suggesting distributed crustal shortening with steeply plunging flow rather than large horizontal displacements (Chardon et al., 1998; Gapais et al., 2005; Cagnard et al., 2007). Analogue models of compression of hot lithospheres produced deformation patterns consistent with observations in Archean granite–greenstone belts and Paleoproterozoic belts and displayed pop-down thrusting of the brittle crust and pure-shear ductile flow of the crust and mantle below (Cagnard et al., 2006).

The steeply dipping foliations as observed in the field will give rise to radial seismic anisotropy with  $V_{SH} < V_{SV}$ . Our measurements of such anisotropy over paths hundreds of kilometers long imply that the distributed crustal shortening with steeply plunging flow may have

occurred over large, regional scales, as has been proposed recently on the basis of the geological data and analogue modelling (Gapais et al., 2005; Cagnard et al., 2006).

#### 5.5. Fabric and anisotropy in the lower crust and upper mantle

In the lower crust–lithospheric mantle depth range, radial anisotropy with  $V_{SH} > V_{SV}$  is preferred or required by the data beneath 9 out of the 10 locations (Table 3). The depth down to which we constrain radial anisotropy beneath most locations is ~100 km, limited by the long-period extent of the Love-wave dispersion curves.

Beneath Western Australia, our long-period data sample deeper and suggest anisotropy ( $V_{SH} > V_{SV}$ ) in the sub-cratonic asthenosphere below ~200 km depth. Gaherty and Jordan (1995) argued that the Lehmann discontinuity at 220 km may represent the bottom of the anisotropic layer beneath continents, which would limit the depth range of anisotropy beneath cratons almost entirely to within the lithosphere. More recently, anisotropy in deep sub-continental asthenosphere has been detected in a number of studies (e.g. Debayle and Kennett, 2000; Gung et al., 2003; Sebai et al., 2006; Pedersen et al., 2006). Beghein and Trampert (2003) concluded that radial anisotropy in the 220–400 km depth range was likely to occur beneath cratons on average. Azimuthal anisotropy in the asthenosphere beneath cratons has also been detected. The close match between the directions of motion of the Australian and North American plates and the directions of fast shear-wave propagation measured in the asthenosphere beneath the plates (Simons et al., 2002; Debayle et al., 2005; Marone and Romanowicz, 2007; Deschamps et al., 2008a,b) represents strong evidence for the plate-motion related flow in the sub-cratonic asthenosphere giving rise to seismic anisotropy.

Arguments against the presence of anisotropy below ~200 km depth invoked the presumed transition from the predominantly dislocation creep above that depth to predominantly diffusion creep below, with the diffusion creep producing nearly no anisotropy (Karato, 1992; Gaherty and Jordan, 1995). Recent high-pressure experiments suggested that dislocation creep may also dominate in the lower part of the upper mantle, albeit with a different slip direction, resulting in extremely low seismic anisotropy below a boundary located at some depth shallower than 330 km (Mainprice et al., 2005). Surface-wave observations would

**Table 3**  
Radially anisotropic structure of Precambrian lithosphere: station pairs; tectonic units sampled; anisotropy in the crust and mantle. “+” stands for anisotropy with  $V_{SH} > V_{SV}$  (indicating horizontally oriented fabric), “-” means anisotropy with  $V_{SH} < V_{SV}$  (vertically oriented fabric), “0” means no anisotropy

No.	Stations	Site	Upper crust	Middle crust	Lower crust	Crustal average	Lithospheric mantle	Average over lower crust and upper lithospheric mantle
1	KEV– –LVZ	Baltic Shield					++ (3–4%)	++
2	PUL– –TRTE –VSU	Russian Platform	0		0		++ (3%)	++
3	MHV– –OBN	Russian Platform	- (2–4%)		+ (3–5%)		+ (3–4%)	++
4	PTGA– –KOG –MPG	Guyana Shield				-	+ (1–1.5%)	++
5	BDFB– –SPB	Paraná Basin	- (3%)		+		++ (3%)	+++
6	BGCA– –MSKU	Congo Craton					+	+
7	MBWA –NWA0	Western Australia					+++	+++
8	BRVK– –KURK	Kazakhstan	– – – (2–3%)	00	+ (1%)		++ (2–3%)	+++
9	KURK– –MAKZ	Kazakhstan	- (1–2%)		+ (1%)		+ (1–2%)	++
10	ENH– –XAN	Yangtze Craton		+	+	+++	0	

“+”, “0”, “-”: anisotropy of this sign or absence of anisotropy is preferred by the data; “+ +”, “00”, “- -”: strongly preferred; “+ + +”, “- - -”: anisotropy of this sign is required by the data. No entry means that anisotropy in this layer at this location is not constrained sufficiently by the present dispersion data for robust conclusions to be derived. The values in parentheses are estimates of the amount of anisotropy,  $|V_{SH} - V_{SV}| / V_{S(ave)}$ .

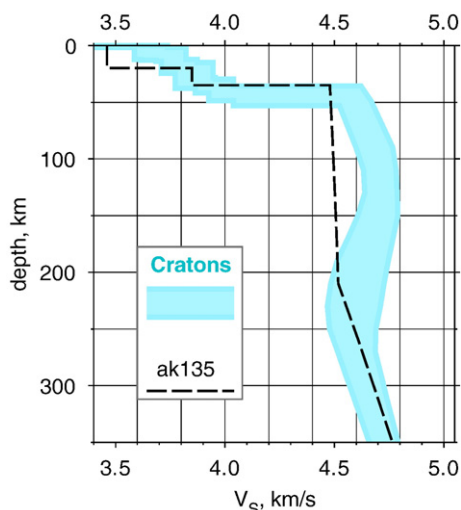


**Fig. 10.** Summary profile of isotropic-average shear speed  $V_S$  beneath cratons. The ranges of  $V_S$  values are determined so that they include the preferred, best-fitting profiles from all the cratonic locations sampled in this study.

be consistent with a strong reduction in the amount of anisotropy at some depth within the asthenosphere. Such reduction, however, would be likely to occur not near 200 km but somewhere below ~250 km depth (Mainprice et al., 2005; Becker et al., 2008).

We interpret the horizontal fabric we detect in the lower crust and mantle lithosphere to be a record of horizontal ductile flow during the deformation episodes before the stabilisation of the cratons. The horizontal fabric and anisotropy below ~200 km reflect the deformation associated with recent asthenospheric flow.

### 6. Conclusions

Figs. 10 and 11 summarise most of our observations and inferences regarding the isotropic and radially anisotropic structure of the lithosphere of cratons.

- (1) An increase in  $V_S$  in the upper ~100 km of the mantle is consistently preferred by the data obtained in this study. It has also featured in seismic models of continents published previously. We argue that this increase can be explained by the transition from the spinel peridotite to garnet peridotite (Hales, 1969) (alternative views are given by Pedersen et al., 2009-this issue). The depth interval of the phase transformation can be tens of kilometers wide and extend down to below

100 km, provided that the bulk Cr/(Cr+Al) ratio is high (Klemme, 2004)—a condition that appears to be met within the depleted cratonic lithosphere, according to a number of xenolith studies (Kopylova and Caro, 2004; Grütter et al., 2006; O'Reilly and Griffin, 2006). Seismic data would be consistent with both a sharp and a gradual (perhaps with a steeper onset) increase in  $V_S$ : a Hales discontinuity or a “Hales gradient”. We argue that the recently reported inconsistency between the observed and calculated seismic velocities in the upper lithosphere (Shapiro and Ritzwoller, 2004; Faul and Jackson, 2005) is largely due to the neglect of the transition from spinel peridotite to garnet peridotite. This transformation needs to be taken into account when relating seismic and thermal structure of the lithosphere.

- (2)  $V_S$  consistently reaches higher values in the lithosphere of cratons than in the lithosphere of Proterozoic foldbelts: on average 5–6% and 2–3%, respectively, above global averages. Because  $V_S$  anomalies of only up to 1% can be attributed to anomalous lithospheric composition (e.g. Deschamps et al., 2002; Schutt and Leshner, 2006), cratonic lithosphere must be substantially colder and, assuming approximately conductive geotherms within the lithosphere, substantially thicker. This is consistent with lithospheric temperature estimates inferred from xenolith and xenocryst data (O'Reilly and Griffin, 2006) and implies that the thermal lithosphere cannot grow as thick beneath Proterozoic foldbelts as it has beneath cratons. A thick, durable, buoyant chemical boundary layer is present beneath cratons but is absent or is thinner beneath the Proterozoic foldbelts (e.g. Jordan, 1988; Griffin et al., 2003).
- (3) Sub-lithospheric mantle beneath continents is thermally heterogeneous: some cratons sampled in this study appear to be underlain by a much hotter asthenosphere than others. Lithospheric seismic velocities, however, reach high values beneath all cratons sampled. Lithospheric geotherms being close to conductive, this confirms that the stable, buoyant lithosphere beneath cratons in general must be substantially thicker than beneath younger units.
- (4) We repeatedly detected radial anisotropy in the upper crust indicative of vertically oriented anisotropic fabric ( $V_{SH} < V_{SV}$ ). We interpret this pattern as a clue on the style of deformation in ancient orogens. Field observations in Archean and Paleoproterozoic transpressive belts yielded evidence for distributed crustal shortening involving steeply plunging flow (Chardon et al., 1998; Gapais et al., 2005; Cagnard et al., 2007). The steeply dipping foliations observed in the field would account for the anisotropy we detected ( $V_{SH} < V_{SV}$ ). Our measurements of this anisotropy over inter-station paths that are hundreds of

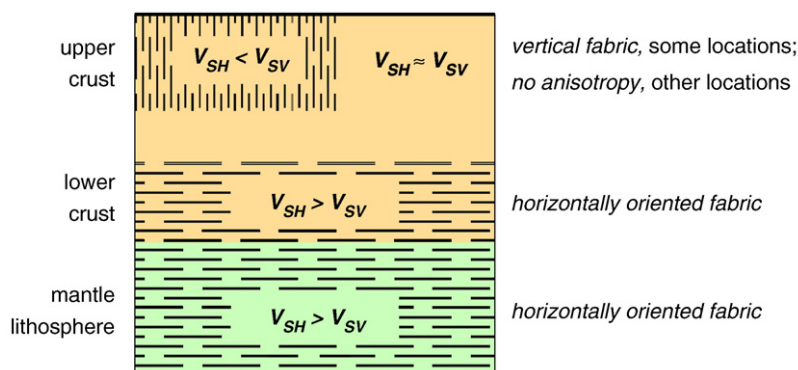


**Fig. 11.** Interpretative summary of the observations of radial anisotropy within the upper Precambrian lithosphere. Anisotropy with horizontally polarised shear waves propagating faster than vertically polarised ones ( $V_{SH} > V_{SV}$ ) is observed in the lower crust and mantle lithosphere and indicates horizontally oriented fabric. Anisotropy with  $V_{SH} < V_{SV}$  is observed in the upper crust beneath some of the locations and suggests the occurrence of vertically oriented fabric.

kilometers long lend support to the view that distributed crustal shortening with sub-vertical flow patterns occurred over large scales in hot ancient orogens (Gapais et al., 2005; Cagnard et al., 2006).

- (5) Radial anisotropy in the lower crust and uppermost mantle was detected in 9 locations out of 10. It is a robust observation and consistently indicates horizontally oriented fabric ( $V_{SH} > V_{SV}$ ). This fabric is likely to be a record of (sub-)horizontal ductile flow in the lower crust and lithospheric mantle at the time of the formation and stabilisation of the cratons.
- (6) We find evidence for radial anisotropy in the 200–400 km depth range beneath the one location (Western Australia) where both our Love and Rayleigh measurements sample down to these depths (this confirms earlier observations of Debayle and Kennett, 2000). Recently, azimuthal anisotropy has also been detected in sub-cratonic asthenosphere beneath both Australia and North America (Simons et al., 2002; Debayle et al., 2005; Marone and Romanowicz, 2007; Deschamps et al., 2008a,b), with the directions of fast shear-wave propagation closely matching those of the plate motions. These results cast doubt on the earlier suggestion that the Lehmann discontinuity (200–220 km depth) may represent the bottom of the anisotropic layer beneath continents (Karato, 1992; Gaherty and Jordan, 1995). Recent observations suggest that deformation related to plate-motion-related mantle flow gives rise to seismic anisotropy in the asthenosphere beneath cratons.

## Acknowledgements

We are grateful to Helle Pedersen, Nicholas Arndt, David Snyder, Don Francis and Tom Jordan for their work on organizing the 2007 workshop “The Structure of the Lithosphere: the Petro-Geophysical Approach”, as well as on editing this volume. We thank Thomas Meier for generously sharing his software and Hanneke Paulssen and Céline Tirel for very helpful discussions. This manuscript benefited from insightful comments by Eric Debayle, Kazu Yoshizawa and Helle Pedersen. Figures were generated with Generic Mapping Tools (Wessel and Smith, 1995). Waveform data was obtained from facilities of the Incorporated Research Institutions for Seismology (IRIS) Data Management System (DMS), funded by the National Science Foundation (NSF). S.L. acknowledges partial support from the VICI Innovative Research Award, awarded to R. D. van der Hilst.

## References

- Argus, D.P., Gordon, R.G., 1991. No-net-rotation model of current plate velocities incorporating plate motion model NUVEL-1. *Geophysical Research Letters* 18, 2039–2042.
- Artemieva, I.M., Thybo, H., Kaban, M.K., 2006. Deep Europe today: geophysical synthesis of the upper mantle structure and lithospheric processes over 3.5 By. In: Gee, D., Stephenson, R. (Eds.), *European Lithosphere Dynamics*. Geophysical Monograph, vol. 32. Geol. Soc. London, pp. 14–41.
- Babuška, V., Montagner, J.P., Plomerová, J., Girardin, N., 1998. Age-dependent large-scale fabric of the mantle lithosphere as derived from surface-wave velocity anisotropy. *Pure and Applied Geophysics* 151, 257–280.
- Bassin, C., Laske, G., Masters, G., 2000. The current limits of resolution for surface wave tomography in North America. *Eos, Transactions - American Geophysical Union* 81, F897.
- Becker, T.W., Kustowski, B., Ekström, G., 2008. Radial seismic anisotropy as a constraint for upper mantle rheology. *Earth and Planetary Science Letters* 267, 213–237.
- Beghein, C., Trampert, J., 2003. Probability density functions for radial anisotropy: implications for the upper 1200 km of the mantle. *Earth and Planetary Science Letters* 217, 151–162.
- Beghein, C., Trampert, J., 2004. Probability density functions for radial anisotropy from fundamental mode surface wave data and the Neighbourhood Algorithm. *Geophysical Journal International* 157, 1163–1174.
- Brune, J., Dorman, J., 1963. Seismic waves and earth structure in the Canadian Shield. *Bulletin of the Seismological Society of America* 53, 167–210.
- Bruneton, M., Pedersen, H.A., Vacher, P., Kukkonen, I.T., Arndt, N.T., Funke, S., Friederich, W., Farra, V., SVEKALAPKO Seismic Tomography Working Group, 2004. Layered lithospheric mantle in the central Baltic Shield from surface waves and xenolith analysis. *Earth and Planetary Science Letters* 226, 41–52.
- Cagnard, F., Brun, J.P., Gapais, D., 2006. Modes of thickening of analogue weak lithospheres. *Tectonophysics* 421, 145–160.
- Cagnard, F., Brun, J.P., Gapais, D., 2007. Collision tectonics involving juvenile crust: the example of the southern Finnish Svecofennides. *Precambrian Research* 154, 125–141.
- Chardon, D., Choukroune, P., Jayananda, M., 1998. Sinking of the Dharwar Basin (South India): implications for Archaean tectonics. *Precambrian Research* 91, 15–39.
- Chevrot, S., Zhao, L., 2007. Multiscale finite-frequency Rayleigh wave tomography of the Kaapvaal Craton. *Geophysical Journal International* 169, 201–215.
- Chevrot, S., Vinnik, L., Montagner, J.P., 1999. Global scale analysis of the mantle  $P$ ds phases. *Journal of Geophysical Research* 104, 20203–20219.
- Debayle, E., Kennett, B.L.N., 2000. Anisotropy in the Australasian upper mantle from Love and Rayleigh waveform inversion. *Earth and Planetary Science Letters* 184, 339–351.
- Debayle, E., Kennett, B.L.N., Priestley, K., 2005. Global azimuthal seismic anisotropy and the unique plate-motion deformation of Australia. *Nature* 433, 509–512.
- Deschamps, F., Lebedev, S., Meier, T., Trampert, J., 2008a. Azimuthal anisotropy of Rayleigh-wave phase velocities in the East-central United States. *Geophysical Journal International* 173, 827–843.
- Deschamps, P., Lebedev, S., Meier, T., Trampert, J., 2008b. Stratified seismic anisotropy reveals past and present deformation beneath the East-central United States. *Earth and Planetary Science Letters*, in revision.
- Deschamps, P., Trampert, J., Snieder, R., 2002. Anomalies of temperature and iron in the uppermost mantle inferred from gravity data and tomographic models. *Physics of the Earth and Planetary Interiors* 129, 245–264.
- Eaton, D.W., Darbyshire, P., Evans, R.L., Grütter, H., Jones, A.G., Yuan, X., 2009. The elusive lithosphere–asthenosphere boundary (LAB) beneath cratons. *Lithos* 109, 1–22 (this issue). doi:10.1016/j.lithos.2008.05.009.
- Ekström, G., 2000. Mapping the lithosphere and asthenosphere with surface waves: lateral structure and anisotropy. In: Richards, M.A., Gordon, R.G., van der Hilst, R.D. (Eds.), *The History and Dynamics of Global Plate Motions*. Geophys. Monograph. AGU, vol. 121, pp. 277–288.
- Endrun, B., Meier, T., Bischoff, M., Harjes, H.P., 2004. Lithospheric structure in the area of Crete constrained by receiver functions and dispersion analysis of Rayleigh phase velocities. *Geophysical Journal International* 158, 592–608.
- Endrun, B., Meier, T., Lebedev, S., Bohnhoff, M., Stavrakakis, G., Harjes, H.P., 2008. Constraints on  $S$  velocity and radial anisotropy in the Aegean region from surface wave dispersion. *Geophysical Journal International*. doi:10.1111/j.1365-246X.2008.03802.x.
- Faul, U.H., Jackson, I., 2005. The seismological signature of temperature and grain size variations in the upper mantle. *Earth and Planetary Science Letters* 234, 119–134.
- Fishwick, S., Reading, A.M., 2008. Anomalous lithosphere beneath the Proterozoic of western and central Australia: a record of continental collision and intraplate deformation? *Precambrian Research*. doi:10.1016/j.precamres.2007.04.026.
- Fishwick, S., Kennett, B.L.N., Reading, A.M., 2005. Contrasts in lithospheric structure within the Australian Craton—insights from surface wave tomography. *Earth and Planetary Science Letters* 231, 163–176.
- Flanagan, M.P., Shearer, P.M., 1998. Global mapping of topography on transition zone velocity discontinuities by stacking SS precursors. *Journal of Geophysical Research* 103, 2673–2692.
- Forste, A.M., Perry, H.C., 2000. Geodynamic evidence for a chemically depleted continental tectosphere. *Science* 290, 1940–1944.
- Fouch, M.J., Rondenay, S., 2006. Seismic anisotropy beneath stable continental interiors. *Physics of the Earth and Planetary Interiors* 158, 292–320.
- Frederiksen, A.W., Bostock, M.G., Cassidy, J.F., 2001.  $S$ -wave velocity structure of the Canadian upper mantle. *Physics of the Earth and Planetary Interiors* 124, 175–191.
- Freybourger, M., Gaherty, J.B., Jordan, T.H., 2001. Structure of the Kaapvaal craton from surface waves. *Geophysical Research Letters* 28, 2489–2492.
- Gaherty, J.B., Jordan, T.H., 1995. Lehmann discontinuity as the base of an anisotropic layer beneath continents. *Science* 268, 1468–1471.
- Gapais, D., Potrel, A., Machado, N., Hallot, E., 2005. Kinematics of long-lasting Paleoproterozoic transpression within the Thompson Nickel Belt, Manitoba, Canada. *Tectonics* 24. doi:10.1029/2004TC001700.
- Grand, S.P., Helmberger, D.V., 1984. Upper mantle shear structure of North America. *Geophysical Journal of the Royal Astronomical Society* 76, 399–438.
- Griffin, W.L., O'Reilly, S.Y., Abe, N., Aulbach, S., Davies, R.M., Pearson, N.J., Doyle, B.J., Kivi, K., 2003. The origin and evolution of Archean lithospheric mantle. *Precambrian Research* 127, 19–41.
- Gripp, A.E., Gordon, R.G., 1990. Current plate velocities relative to the hotspots incorporating the NUVEL-1 global plate motion model. *Geophysical Research Letters* 17, 1109–1112.
- Grütter, H., Latti, D., Menzies, A., 2006. Cr-saturation arrays in concentrate garnet compositions from kimberlite and their use in mantle barometry. *Journal of Petrology* 47, 801–820.
- Gung, Y., Panning, M., Romanowicz, B., 2003. Global anisotropy and the thickness of continents. *Nature* 422, 707–711.
- Hales, A.L., 1969. A seismic discontinuity in the lithosphere. *Earth and Planetary Science Letters* 7, 44–46.
- Heintz, M., Debayle, E., Vauchez, A., 2005. Upper mantle structure of the South American continent and neighboring oceans from surface wave tomography. *Tectonophysics* 406, 115–139.
- Jordan, T.H., 1975. The continental tectosphere. *Reviews of Geophysics and Space Physics* 13, 1.
- Jordan, T.H., 1988. Structure and formation of the continental tectosphere. *Journal of Petrology Special Lithosphere Issue*, pp. 11–37.
- Karato, S.I., 1992. On the Lehmann discontinuity. *Geophysical Research Letters* 19, 2255–2258.

- Kennett, B.L.N., Engdahl, E.R., Buland, R., 1995. Constraints on seismic velocities in the Earth from traveltimes. *Geophysical Journal International* 122, 108–124.
- Klemme, S., 2004. The influence of Cr on the garnet–spinel transition in the Earth's mantle: Experiments in the system MgO–Cr<sub>2</sub>O<sub>3</sub>–SiO<sub>2</sub> and thermodynamic modelling. *Lithos* 77, 639–646.
- Kopylova, M.G., Caro, G., 2004. Mantle xenoliths from the Southeastern Slave craton: evidence for chemical zonation in a thick, cold lithosphere. *Journal of Petrology* 45, 1045–1067.
- Kuskov, O.L., Kronrod, V.A., Annersten, H., 2006. Inferring upper-mantle temperatures from seismic and geochemical constraints: implications for Kaapvaal craton. *Earth and Planetary Science Letters* 244, 133–154.
- Lebedev, S., Nolet, G., 2003. Upper mantle beneath Southeast Asia from S velocity tomography. *Journal of Geophysical Research* 108. doi:10.1029/2000JB000073.
- Lebedev, S., van der Hilst, R.D., 2008. Global upper-mantle tomography with the automated multimode inversion of surface and S wave forms. *Geophysical Journal International* 173, 505–518.
- Lebedev, S., Chevrot, S., van der Hilst, R.D., 2002. Seismic evidence for olivine phase changes at the 410- and 660-kilometer discontinuities. *Science* 296, 1300–1302.
- Lebedev, S., Chevrot, S., van der Hilst, R.D., 2003. Correlation between the shear-speed structure and thickness of the mantle transition zone. *Physics of the Earth and Planetary Interiors* 136, 25–40.
- Lebedev, S., Meier, T., van der Hilst, R.D., 2006. Asthenospheric flow and origin of volcanism in the Baikal Rift area. *Earth and Planetary Science Letters* 249, 415–424.
- Lebedev, S., Nolet, G., Meier, T., van der Hilst, R.D., 2005. Automated multimode inversion of surface and S waveforms. *Geophysical Journal International* 162, 951–964.
- Lee, C.T.A., Lenardic, A., Cooper, C.M., Niu, F.L., Levander, A., 2005. The role of chemical boundary layers in regulating the thickness of continental and oceanic thermal boundary layers. *Earth and Planetary Science Letters* 230, 379–395.
- Levshin, A., Ratnikova, L., 1984. Apparent anisotropy in inhomogeneous media. *Geophysical Journal of the Royal Astronomical Society* 76, 65–69.
- Levshin, A.L., Schweitzer, J., Weidle, C., Shapiro, N.M., Ritzwoller, M.H., 2007. Surface wave tomography of the Barents Sea and surrounding regions. *Geophysical Journal International* 170, 441–459.
- MacGregor, I.D., 1970. The effect of CaO, Cr<sub>2</sub>O<sub>3</sub>, Fe<sub>2</sub>O<sub>3</sub> and Al<sub>2</sub>O<sub>3</sub> on the stability of spinel and garnet peridotites. *Physics of the Earth and Planetary Interiors* 3, 372–377.
- Mainprice, D., Tommasi, A., Couvy, H., Cordier, P., Frost, D.J., 2005. Pressure sensitivity of olivine slip systems and seismic anisotropy in the Earth's upper mantle. *Nature* 433, 731–733.
- Marone, F., Romanowicz, B., 2007. The depth distribution of azimuthal anisotropy in the continental upper mantle. *Nature* 447, 198–201.
- Marshak, S., 1999. Deformation style way back when: thoughts on the contrasts between Archean/Paleoproterozoic orogens and modern ones. *Journal of Structural Geology* 21, 1175–1182.
- Meier, T., Dietrich, K., Stockhert, B., Harjes, H.P., 2004. One-dimensional models of shear wave velocity for the eastern Mediterranean obtained from the inversion of Rayleigh wave phase velocities and tectonic implications. *Geophysical Journal International* 156, 45–58.
- Meissner, R., Rabbela, W., Kern, H., 2006. Seismic lamination and anisotropy of the lower continental crust. *Tectonophysics* 416, 81–99.
- O'Reilly, S.Y., Griffin, W.L., 2006. Imaging global chemical and thermal heterogeneity in the sub-continental lithospheric mantle with garnets and xenoliths: geophysical implications. *Tectonophysics* 416, 289–309.
- Paulssen, H., 1987. Lateral heterogeneity of Europe's upper mantle as inferred from modeling of broad-band body waves. *Geophysical Journal of the Royal Astronomical Society* 91, 171–199.
- Pedersen, H.A., 2006. Impacts of non-plane waves on two-station measurements of phase velocities. *Geophysical Journal International* 165, 279–287.
- Pedersen, H.A., Bruneton, M., Maupin, V., SVEKALAPKO Seismic Tomography Working Group, 2006. Lithospheric and sublithospheric anisotropy beneath the Baltic Shield from surface-wave array analysis. *Earth and Planetary Science Letters* 244, 590–605.
- Pedersen, H.A., Fishwick, S., Snyder, D.B., 2009. A comparison of cratonic roots through consistent analysis of seismic surface waves. *Lithos* 109, 81–95 (this issue).
- Petitjean, S., Rabinowicz, M., Grégoire, M., Chevrot, S., 2006. Differences between Archean and Proterozoic lithospheres: assessment of the possible major role of thermal conductivity. *Geochemistry, Geophysics, Geosystems* 7. doi:10.1029/2005GC001053.
- Priestley, K., McKenzie, D., 2006. The thermal structure of the lithosphere from shear wave velocities. *Earth and Planetary Science Letters* 244, 285–301.
- Reinecker, J., Heibach, O., Tingay, M., Sperner, B., Muller, B., 2005. The 2005 release of the World Stress Map. [www.world-stress-map.org](http://www.world-stress-map.org).
- Revenaugh, J., Jordan, T.H., 1991. Mantle layering from ScS reverberations: 3. The upper mantle. *Journal of Geophysical Research* 96, 19781–19810.
- Ritsema, J., van Heijst, H.J., Woodhouse, J.H., 2004. Global transition zone tomography. *Journal of Geophysical Research* 109. doi:10.1029/2003JB002610.
- Sambridge, M., 1999a. Geophysical inversion with a Neighbourhood Algorithm-I. Searching a parameter space. *Geophysical Journal International* 138, 479–494.
- Sambridge, M., 1999b. Geophysical inversion with a Neighbourhood Algorithm-II. Appraising the ensemble. *Geophysical Journal International* 138, 727–746.
- Schutt, D.L., Leshner, C.E., 2006. Effects of melt depletion on the density and seismic velocity of garnet and spinel lherzolite. *Journal of Geophysical Research* 111. doi:10.1029/2003JB002950.
- Sebai, A., Stutzmann, E., Montagner, J.P., Sicilia, D., Beucler, E., 2006. Anisotropic structure of the African upper mantle from Rayleigh and Love wave tomography. *Physics of the Earth and Planetary Interiors* 155, 48–62.
- Shapiro, N.M., Ritzwoller, M.H., 2002. Monte-Carlo inversion for a global shear velocity model of the crust and upper mantle. *Geophysical Journal International* 151, 88–105.
- Shapiro, N.M., Ritzwoller, M.H., 2004. Thermodynamic constraints on seismic inversions. *Geophysical Journal International* 157, 1175–1188.
- Simons, F.J., van der Hilst, R.D., Montagner, J.P., Zielhuis, A., 2002. Multimode Rayleigh wave inversion for shear wave speed heterogeneity and azimuthal anisotropy of the Australian upper mantle. *Geophysical Journal International* 151, 738–754.
- Sleep, N.H., 2003. Fate of mantle plume material trapped within a lithospheric catchment with reference to Brazil. *Geochemistry, Geophysics, Geosystems* 4. doi:10.1029/2002GC000464.
- Snoke, J.A., James, D.E., 1997. Lithospheric structure of the Chaco and Paraná basins of South America from surface-wave inversion. *Journal of Geophysical Research* 102, 2939–2951.
- Stixrude, L., Lithgow-Bertelloni, C., 2005. Mineralogy and elasticity of the oceanic upper mantle: origin of the low-velocity zone. *Journal of Geophysical Research* 110. doi:10.1029/2004JB002965.
- Van der Lee, S., Nolet, G., 1997. Upper-mantle S-velocity structure of North America. *Journal of Geophysical Research* 102, 22,815–22,838.
- Wessel, P., Smith, W.H.F., 1995. New version of the Generic Mapping Tools released. *Eos, Transactions - American Geophysical Union* 76, 329.
- Yoshizawa, K., Kennett, B.L.N., 2004. Multimode surface wave tomography for the Australian region using a three-stage approach incorporating finite frequency effects. *Journal of Geophysical Research* 109. doi:10.1029/2002JB002254.
- Zielhuis, A., Nolet, G., 1994. Deep seismic expression of an ancient plate boundary in Europe. *Science* 265, 79–81.